Thorium, europium and s-process elements in Galactic halo vs. Gaia-Enceladus

Stefan Kuipers
Under supervision of E. Tolstoy, J. Even and Á. Skúladóttir

1 June 2021

Abstract

In this thesis I have measured the abundances of a range of chemical elements, including heavy r-process elements europium and thorium in a group of 6 stars in the Milky Way, selected from the sample of Nissen & Schuster 2010. My sample includes 4 halo stars, of which 2 are likely to be from the dwarf galaxy Gaia Enceladus that merged with the Milky Way around 10 Gyr ago, and also includes 2 stars which are likely from the thick disk of the Milky Way. This is the first time that Th has been detected in any of these stars.

The analysis was carried out on high spectral resolution, high signal-to-noise VLT/UVES spectra, using spectral synthesis, and the spectral parameters (T_{eff}, log g, ξ_{turb}) determined by Nissen & Schuster. There are differences between my results and those of Nissen & Schuster but the general characteristics of the sample remain the same and are consistent with the results presented by Nissen & Schuster. I have found that Gaia-Enceladus stars have lower [Mg/Fe] than either the other 2 halo stars or the thick disk stars, in agreement with Nissen & Schuster. In addition I show that [Eu/Mg] is higher in Gaia-Enceladus stars, which indicates enhanced r-process enrichment. However [Th/Fe] and the other elements I have measured are remarkably similar for all the 6 stars. This shows that the differences in chemical properties of my sample of stars with 3 different origins are subtle.

1 Introduction

Aside from a few of the lightest elements, all elements in our universe are created in stars or stellar remnants. During most of their lifetime, stars are burning hydrogen to form helium via either the pp-chain or the CNO cycle [1]. However, when stars enter the final stages of their life, the more interesting elements in our universe are created. It is these heavy elements that are the topic of this thesis.

1.1 Stellar burning

In the cores of main sequence stars, hydrogen nuclei are being fused into helium nuclei via two different processes. In the proton-proton chain (pp-chain), individual protons and other low mass nuclei like ^{2}H, ^{3}He are fused together until eventually ^{4}He is formed. In CNO cycles, elements like ^{12}C, ^{14}N and ^{16}O are fused with protons until they eventually decay back to the original nuclei via emission of an ^{4}He nucleus.[1] While individual CNO cyles and pp-chains are different, the resulting reaction is always the same:

$$4p \rightarrow {}^{4}\mathrm{He} + 2e^{+} + 2\nu. \tag{1}$$

Towards the end of their life, when their hydrogen fuel is gone, the core of the heavier stars contract and heat up until they are able to start to burn helium instead of hydrogen. This process forms carbon and oxygen. When the helium is exhausted and the star contracts further, those elements themselves are burned to form even heavier elements.[1] This continues until the stars are left with iron peak elements in their core. As fusion beyond iron does not create energy anymore, the star collapses and explodes as a supernova. The elements that are formed both in the star as well as in the resulting explosion this way are mostly the α elements and the iron peak elements. α elements are elements with a stable isotope whose nucleus can be made by an integer amount of ^{4}He nuclei, like Ne, Mg, Si, S, Ar and Ca. However, although stellar fusion does not produce many elements heavier than iron, those elements are produced in the supernova explosion by neutron capture. The two main processes that produce these heavy elements are called the slow neutron-capture process (s-process) and the rapid-neutron capture process r-process.

1.2 Neutron capture processes

The s-process, or the slow neutron capture process, happens most often in the outer layers of AGB stars. During this process, nuclei slowly capture free neutrons over time. If the nucleus becomes unstable due to the extra neutron, it decays through beta minus decay back toward the valley of stability. Beta minus decay is the emission of electron with an anti-neutrino by the atom. In case of the s-process, the beta-decay timescales are shorter than the timescales for neutron capture, which results in almost any unstable nucleus decaying before capturing another neutron. Via this process, the nulcei slowly become heavier until either the neutron supply dries up, or they eventually form lead and bismuth. As all elements heavier than those are unstable and decay back towards lead via emission of an α-particle, the s-process is unable to form any heavier elements[1].

Something else that affects the abundance of neutron capture isotopes is the neutron magic numbers. Elements with certain neutron numbers, which include 50, 82 and 126, have energetically favourable configurations. Due to this, the neutron-capture cross section decreases and the capture rates therefore decrease. In Figure 1, we clearly see a peak in abundance around the elements with magic neutron numbers, indicated by 's-process peak', which is explained by their increased stability.

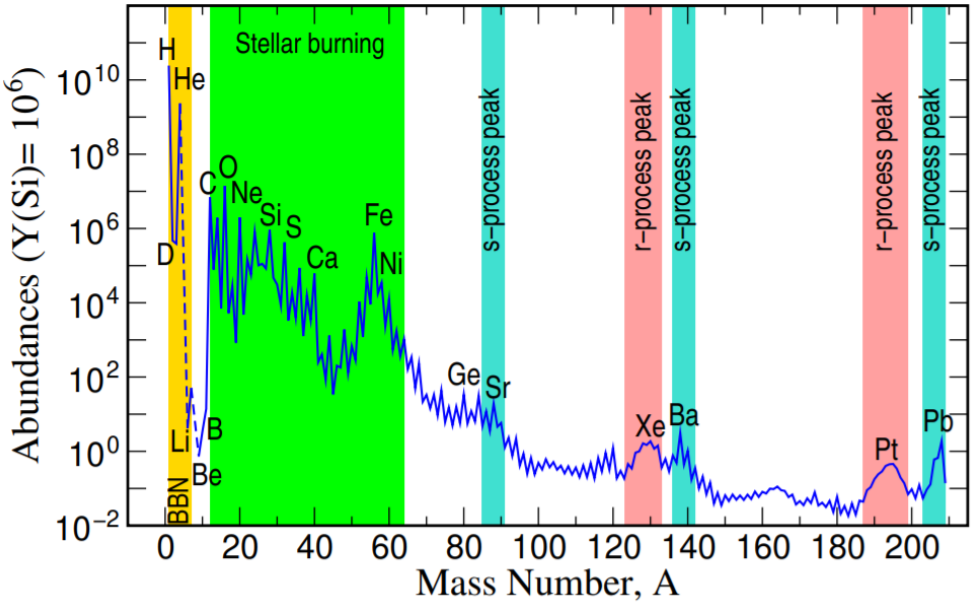

Figure 1: The abundance of the heavy nucleids in our solar system as a function of mass number[2]. The main s and r process peaks are indicated.

In contrast to the s-process, the r-process experiences an extremely high neutron flux. Therefore, unstable nuclei often do not have the time to decay before they capture another neutron. This results in the r-process initially producing nuclides with far more neutrons than the s-process, as can be seen in Figure 2.

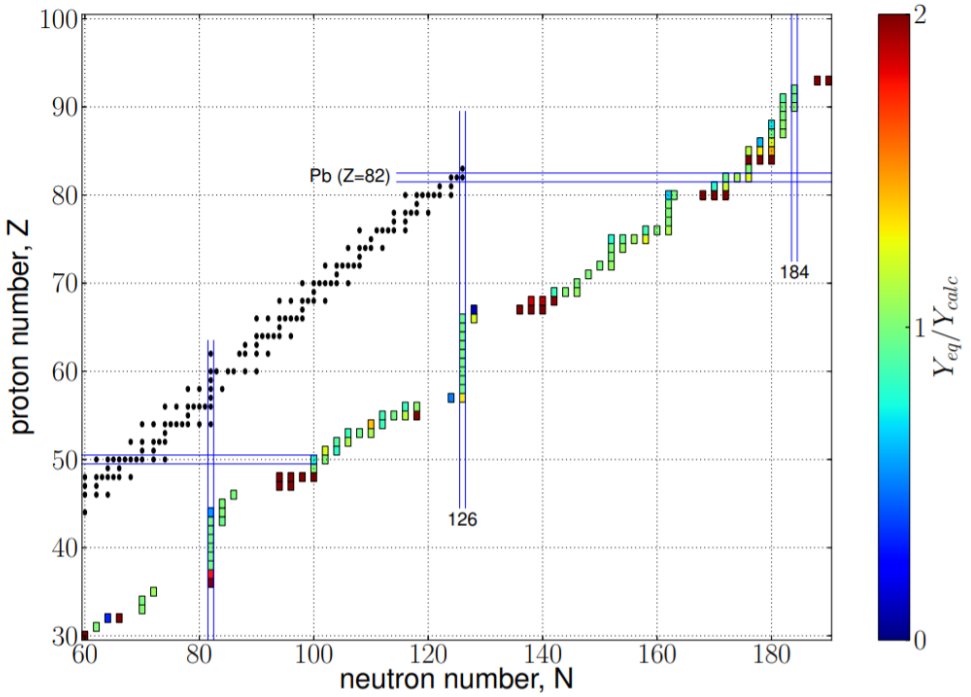

Figure 2: An example of an r-process path, given by the coloured squares [2]. The stable isotopes are given by black squares. The closer the color is to 1, the better the model works.

Like in the s-process, the nuclides in the r-process tend towards having magic neutron numbers. That happens because around these magic neutron numbers, the competing neutron flux and photo-disintegration reactions are in equilibrium. Because of that, the points in the r-process with the magical neutron numbers of 50, 82 and 126 are also called the 1st, 2nd and 3rd waiting point. In contrast to the s-process, when the neutron flux stops, all the formed nuclides from the r-process quickly start to beta-decay back towards the valley of stability. The elements that are eventually formed from the decaying magic neutron number elements are a bit lighter than the s-process elements with the same original magic neutron numbers. Hence all s-process abundance peaks are accompanied by a r-process abundance peak at slightly lower mass numbers, which is clearly visible for the second and third s-process peaks in Figure 1.

What is unique for the r-process, is that it is able to create elements heavier than the termination point through alpha-decay, which the s-process is unable to do. The most notable of these elements are thorium and uranium, because of the long half lives of their most stable isotopes. Due to their spot on the periodic table, these elements are called actinides.

Figure 3 shows the periodic table indicating the synthesis processes of the elements, and lets us see which heavy elements are created by the s-process and which elements are created by the r-process. Note that all elements heavier than iron with dying low mass stars as their origin are created by the s-process in AGB stars.

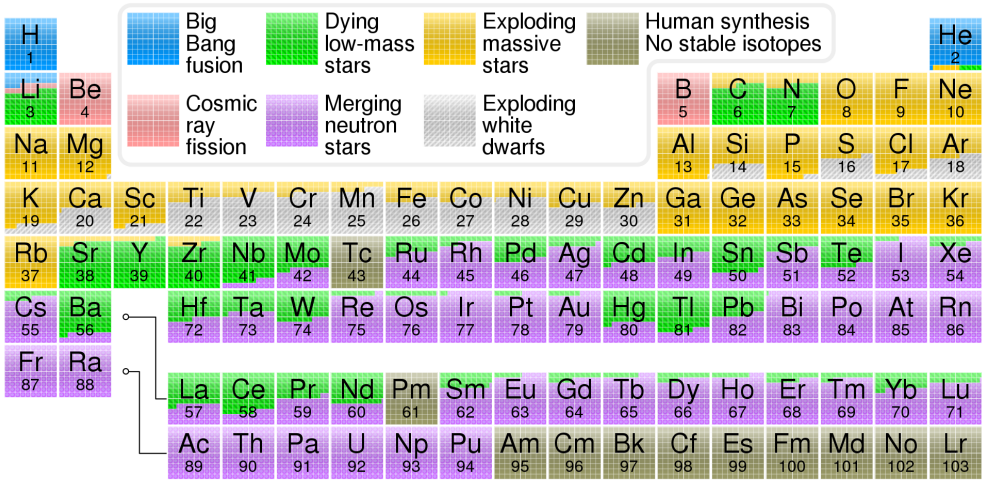

Figure 3: Periodic table of the elements. The color code indicates the fomation of elements. [3].

From Figure 3, we observe that most elements from strontium onward are at least partially created by the s-process, with the notable exception of the elements heavier than bismuth. However, it is also clearly visible that the proportion of s-process elements created is variable.

Part of the variability can be explained by the way the s-process works. The s-process follows an almost fixed path along the valley of stability, an example of which can be observed in Figure 4. Only if the decay time of an isotope along a path is similar to the neutron collision rate will the s-process stray from the path with a reasonable probability [1]. However, from Figure 4, we can clearly see that some isotopes like ^{160}Gd and ^{158}Dy are not reached by the s-process. If none of the stable isotopes is easily reached by the s-process, while they are reached by the r-process, then the origin of this element will be pure r-process. In contrast, if the isotopes are unreachable by the r-process like ^{160}Dy, but they are on the s-process path, than the origin will be pure s-process.

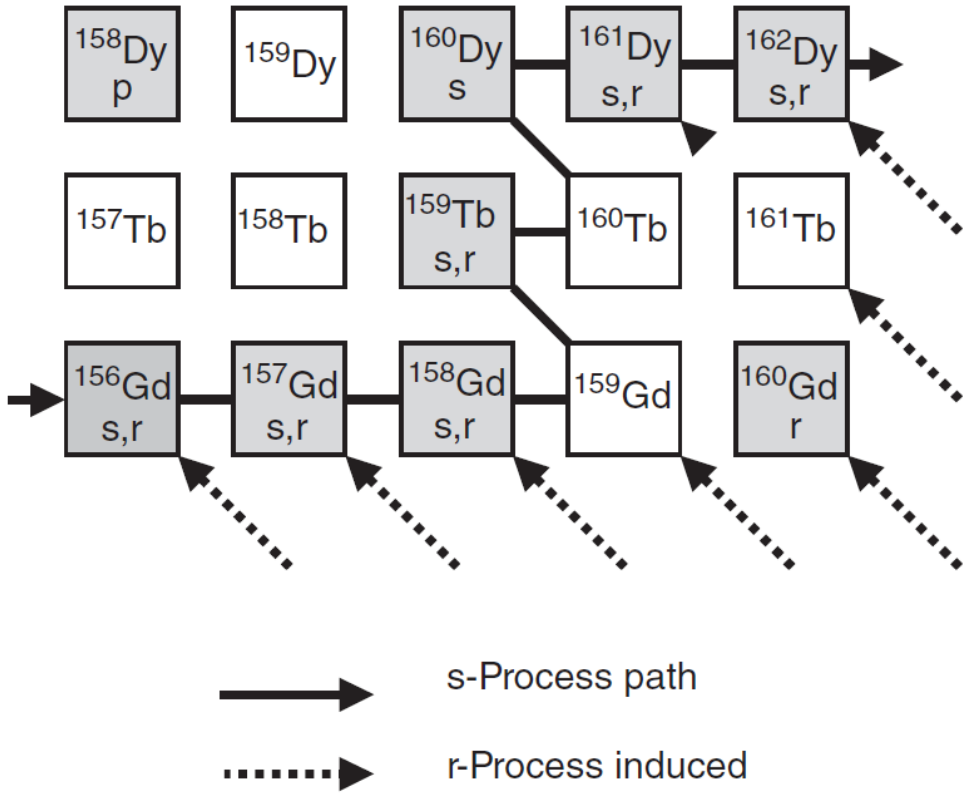

Figure 4: An example of an s-process path [1]. Nuclides reached by the s-process are labeled s and nuclides reached by the r-process are labeled r. Nuclides that are reached by neither are labeled p.

Due to the nature of the r-process, there exist certain isotopes that cannot be created. This is because the r-process always results in nuclides with too many neutrons, which will then beta decay towards the valley of stability. Hence, if a stable isotope is 'shielded' from beta decay by another isotope with the same mass number but lower proton count, then it is impossible for the r-process to create this isotope. In Figure 4, ^{160}Dy is an example for such an isotope, as it is shielded by ^{160}Gd. Note that some of those isotopes are also shielded from the s-process, like ^{158}Dy. These isotopes are therefore only reachable by proton capture processes, namely the p-process and rp-process, which won't be discussed in this thesis.

There is no obvious single source for the r-process. Originally, the innermost ejecta of core-collapse supernovae were believed to be the main origin of the process [4]. However, recent studies show that at most a weak r-process can occur under these conditions [5], which would not be enough to create a significant abundance for the third r-process peak and the actinides. Nowadays, neutron star mergers are instead believed to be an important source of the r-process [2]. However, research has shown that they are not the only source of heavier r-process elements [6]. The outer layers of supernova explosions [7] and core-collapse events of massive stars with fast rotation and high magnetic fields [2] have also been suggested as possible r-process sites, although the first one cannot explain our solar r-process pattern [8].

1.2.1 The i-process

Aside from the s-process and r-process, both of which have been confirmed by observations, there is also a theoretical third neutron-capture process. This is called the intermediate process, or i-process. In the i-process, the neutron flux is stronger than in the s-process, but weaker than in the r-process and therefore moves along a unique path. Notably, the i-process can explain the abundance ratios found in certain carbon-enhanced metal poor stars, where some stars have high heavy to low s-process element ratios but at the same time low [La/Eu] ratios [9]. One site where the i-process can occur is in post-AGB stars during the Very Late Thermal Pulse H-ingestion event [10].

1.3 Galactic archaeology

Galactic archaeology is the subject of investigating stars, stellar remnants, gas and other cosmological structures today to uncover the history of the nearby universe [11]. What is notable for this field is that the abundance of elements in stellar photospheres is constant for most elements over time, being equal to the abundances in the gas out of which the star formed. Fusion inside the core of the star does not affect these outer layers. Because of this,

by looking at the abundances of stars now, we are essentially looking at the abundances in the local neighbourhood when the star was formed. As many stars are more then 10 Gyr old, this allows us to determine the conditions of the local universe far into the past. Therefore, the abundances of the stars I am observing in this thesis are indicators of the ancient history of the Milky Way.

1.4 Nissen and Schuster

In this thesis, we are mostly interested in the heavy r-process elements. Especially thorium and uranium. However, to find these elements, a high signal to noise ratio and high spectral resolution of the stellar spectrum is needed. The sample chosen is from the 2010 Nissen and Schuster paper (noted as NS10) [12]. They analyzed a sample from our solar neighbourhood which consisted of stars mostly from our Galactic halo, although including a few stars from the thick disk of the Milky Way. They found out that the local Galactic halo consisted of two clearly distinguishable populations. One of which had a lower abundance of α-elements than the other, which was comparable to the thick disk stars. In Figure 5, the results from Nissen and Schuster are shown and the two different populations are clearly visible, and plotted in red and blue for clarity.

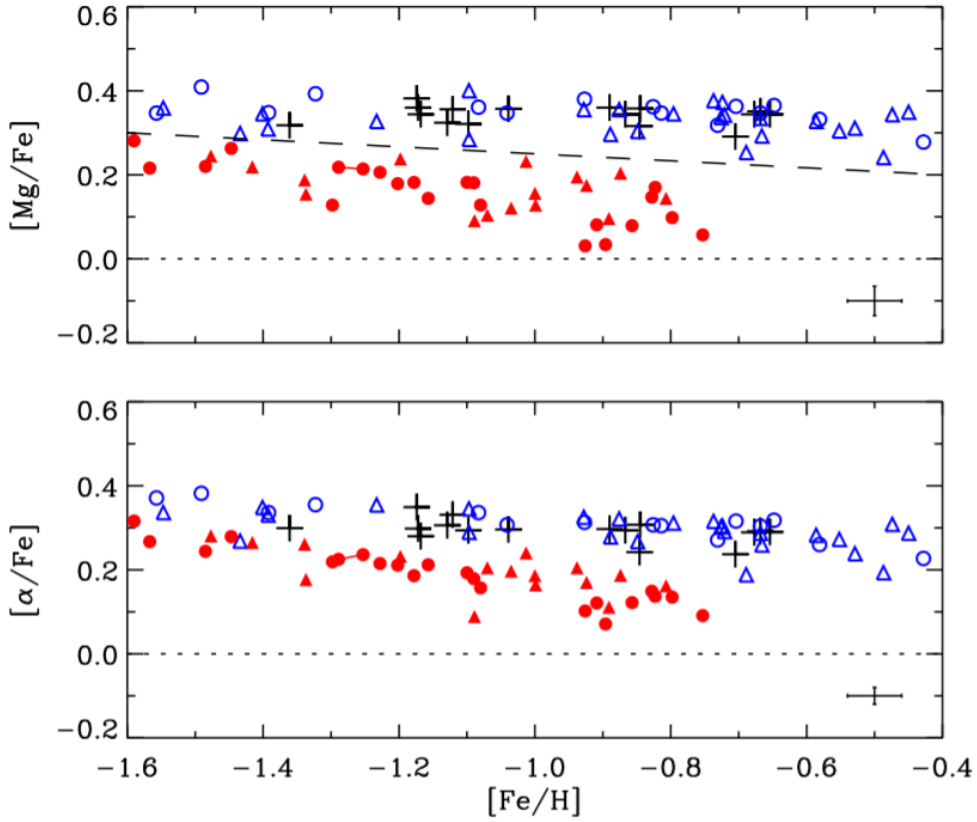

Figure 5: The magnesium and α-element abundances taken as the average of Mg, Ca, Si and Ti, are plotted against the iron abundance from Nissen and Schuster [12]. The blue symbols denote the high-α population, the red symbols denote the low-α population, and the black plusses denote the thick disk stars

In Figure 6, the kinematics of the stars are plotted in a Thoomre diagram. A Thoomre diagram plots the orbital velocity against the velocity perpendicular to Galactic rotation and can be used to compare kinematics of stars. We see a distinct difference between the kinematics of the two halo populations.

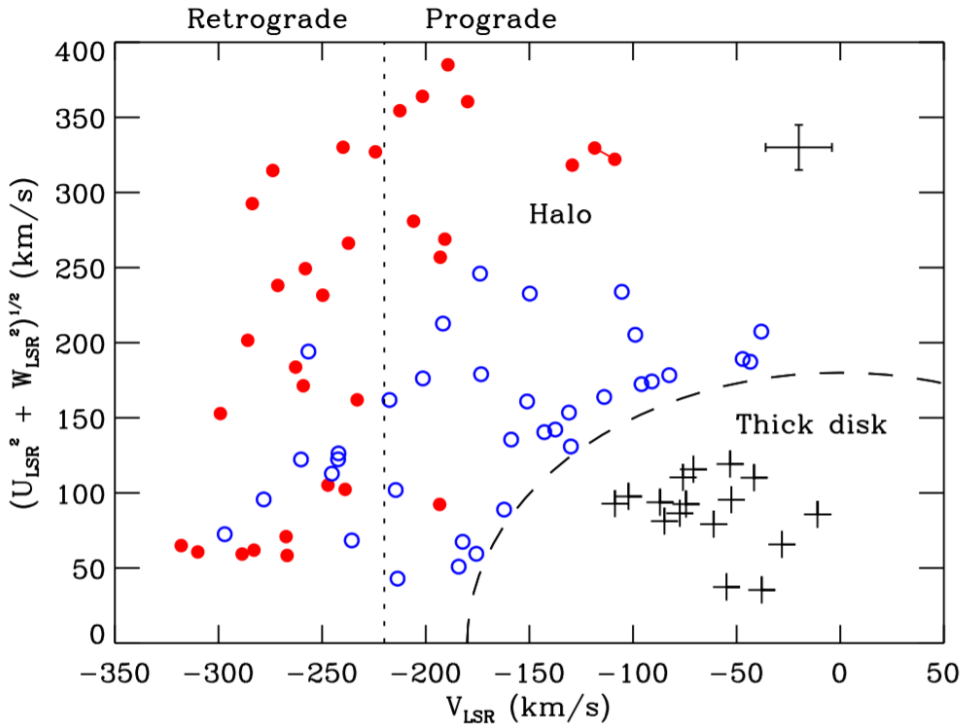

Figure 6: The kinematics for the stars in the Nissen and Schuster paper are plotted in a Toomre diagram [12]. The x-axis denotes the orbital velocity while the y-axis denotes the velocity perpendicular to Galacitc rotation. The blue symbols denote the high-α population, the red symbols denote the low-α population, and the black plusses denote the thick disk stars.

In the paper, based upon the Toomre diagram, Nissen and Schuster concluded that the low-α stars originate from at least one other dwarf galaxy.

The next year, Nissen and Schuster published another paper using the same stars where they observed the elements Mn, Cu. Zn, Y and Ba (noted as NS11) [13]. They did find systematic differences in [Cu/Fe], [Zn/Fe] and [Ba/Y] for the high and low-α stars, adding further proof that they were indeed dealing with separate populations. However, they notably did not find a systematic difference in [Ba/Fe] between the two groups.

Other papers have futher studied the same sample of stars as the NS10 paper. For some stars, Fishlock et al [14] measured the abundances of some neutron capture elements, most notably europium and lanthanum. From their research, they concluded that there was no clear difference in [La/Fe] between the groups of stars and that it also didn't seem to be dependent on the metalicity. However, they did find that low-α stars seem to have a slightly higher [Eu/Fe] than the high-α stars, and that the low-α group showed a potential decrease in Eu with increasing metalicity. However, their sample size was not large enough to fully confirm that. Using results from the NS11 paper [13], they did however confirm that the [Ba/Eu] abundance ratio was lower in low-α stars compared to high-α stars.

Both in the paper by Ge et al (2016)[15], as well as in another follow-up by Nissen & Schuster in 2012 [16] the ages of the stars in the NS10 sample have been estimated. This was done using the carbon and oxygen abundance of said stars combined with stellar models in the first case, and using isochrones from Y^2 models utilizing the iron and α-element abundances in the second case. They found that the low-α stars are on average 2.0 Gyr younger than the high-α stars. The average age of the thick disk stars was somewhere in between, although with more variation, indicating a longer star formation phase.

In the Gaia data release 2, the work of Nissen & Shuster was confirmed. There were indeed two uniquely identifyable populations within the galactic halo. A clear merger between the Milky way and another galaxy was confirmed. This former dwarf galaxy, which includes the low-α stars from NS10, is called Gaia-Encaladus [17]. It was later determined that said galaxy was slightly more massive than the Large Magellanic cloud at the time of collision. At that time, about 10 Gyr ago, the Milky Way itself was just 4 times larger than said dwarf galaxy. This merger ended up contributing significantly to the formation of the current thick disk of the Milky Way [18].

Futher studies of the Gaia-Encaladus stars have been made. In a paper from Matsuno et al (2021) [19], more stars suspected to originate from the same galaxy as the low-α stars selected from Gaia have been used to gain further insight into the origin of the r-process elements in this (dwarf)galaxy. They found a high [Eu/Mg] ratio for

the stars, as well as unenhanced [Ba/Eu] & [La/Eu] ratios indicating a lack of significant s-process contribution for the events that created the high [Eu/Mg] ratio. the paper concluded that the high [Eu/Mg] ratio could be explained by r-process enrichment from neutron star mergers.[19]

While Gaia-Encaladus has an enhanced r-process abundance, that is not a necessity for dwarf galaxies in general. Skúladóttir et al (2019) [20] analyzed the Sculptor dwarf galaxy and found [Eu/Mg] ratios similar to the Milky Way. In Figure 7, we see that the [Eu/Mg] ratios of the Sculptor stars are similar to those of the Milky Way, indicating a lack of r-process enhancement in Sculptor.

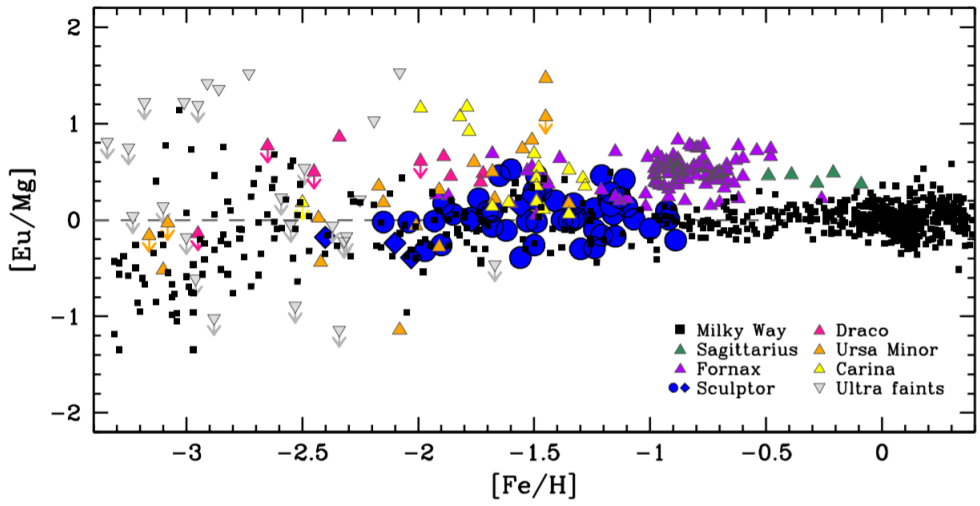

Figure 7: The [Eu/Mg] ratios of stars in different Local Group galaxies against the metallicity of said stars. Copied from the 2019 paper by Á. Skúladóttir et al [20]

Gaia-Encaladus is not the only dwarf galaxy captured by the Milky Way. Sagittarius is a dwarf spheroidal galaxy which is still in the process of being stripped apart by the Milky Way. In Hansen et al (2018) [21], the authors analyzed a group of very metal poor stars in the main body of Sagittarius. As their analysis includes the same elements as those in this thesis, we can compare the results and see whether there are differences in the abundances of the Sagittarius stars and the Gaia-Encaladus stars and what that can tell us about the less well known history of Gaia-Encaladus. According to Hansen et al (2018), most of the Sagittarius stars have been enhanced by a range of AGB stars with a range of masses between 1.3 and 5 $M_{\odot}$

1.5 Observing heavy r-process elements

Thorium and uranium are unstable elements that decay over time and so their abundances can be used to determine the age of the r-process event that created them [22]. If the abundance of another r-process element with the same origin is known, then their ratio is only dependent on the age of the event. However, one first needs to know for sure that the r-process element being compared is always produced with the same ratio with respect to thorium or uranium and what exactly said ratio is.
In the paper of Ji & Freibel (2018) [22], they stated that the age of the r-process event could be derived from:

$$age = 46.67[log(Th/r)_{initial} - log(Th/r)_{now}] \tag{2}$$

which was obtained using using the half life of ^{232}Th, where r is the abundance of the stable r-process element, usually europium. However, as the half-life is $1.4 * 10^{10}$ years, the estimation ends up extremely sensitive to small errors in the thorium measurement and the initial [Th/Eu] production ratio.

In case of uranium, the lower half life of ^{238}U makes the resulting age less sensitive to errors in the uranium measurement. The age is calculated using the following formula[23]:

$$age = 14.8[log(U/r)_{initial} - log(U/r)_{now}] \tag{3}$$

The main caveat here is that measuring the uranium abundance is much harder than measuring thorium, especially when high accuracy is desired as the atmospheric lines are extremely weak and blended.

Finally, the abundance ratio of thorium and uranium [U/Th] can also be used to determine the age. Goriely & Clairbaux (1999)[24] claimed that this ratio is a better way of calculating the age than using [Th/Eu] because the mass difference between Th and U is negligible, making it far more likely that the production ratio between

the two elements is independent of the event that created them. As both elements are unstable, a different formula for age is necessary[23]:

$$age = 21.8[log(U/Th)_{initial} - log(U/Th)_{now}] \quad (4)$$

Of course, this way of calculating the age has the same disadvantage as using [U/Eu], namely the difficulty in measuring uranium abundance.

Heavy elements can also be used to confirm or deny the universality of the r-process. If r-process events would always produce elements with the same abundance ratio between them, then the observed abundance ratio between Th and the other r-process elements would only depend on the age of the event. In the paper of Yushchenko et al (2005) [25], they confirmed that [Th/Eu] varied more in between different stars than could be explained by just a difference in age. Hence, they confirmed that r-process events do not always produce a unique [Th/Eu] abundance. Unfortunately, this also makes using that ratio to determine the age of an r-process event more unreliable.

2 Spectroscopy

To find out the abundances of chemical elements in stars, we make use of spectroscopy. When light passes through a plasma, it can get absorbed by chemical elements if it approximately has the wavelength that corresponds to the energy needed for the transition of an electron from one shell to another. Hence, if multiple photons containing a large range of wavelengths pass through a plasma, the observed spectrum will have dips corresponding to the transition wavelengths of the elements found in the plasma with transitions in the used wavelength range. Those dips are called absorption lines.

This is the situation in stars, where photons from a large range of wavelengths leave the star through the photosphere. The elements in the stellar atmosphere absorb the photons around the transition wavelengths, which leaves the stellar spectrum we observe on Earth filled with absorption lines. The depth of said absorption lines depends on multiple variables, like the temperature, surface gravity and micro-turbulence of the star. However, more importantly, the size of the lines is directly dependent on the abundance of the corresponding element. Therefore, if all stellar parameters are taken into account, it becomes theoretically possible to derive the abundance of the individual elements in the stellar photosphere.

In order to take into account the stellar parameters, a model of the stellar atmosphere and its effect on the spectra is needed. Once a suitable model if found, one can use that to make a synthetic spectrum and find the abundances by comparing it to the real spectrum. In section 5, this will be explained further.

To find the the strongest absorption lines of my stars, I used the NIST handbook of Basic Spectroscopic Data [26].

3 Data collection and corrections

3.1 UVES

In this thesis, a small subgroup of 6 stars from the sample analysed by Nissen and Schuster (NS10)[12] will be used, which are selected because they have high signal to noise (S/N) ratios and therefore offer the highest probability to measure thorium and uranium. The wavelength range analyzed for these stars is in between 3730 and 4400Å.

The spectra of these stars come from the ESO VLT/UVES instrument, and can be accessed using the public ESO archive [27]. UVES is a high resolution optical spectograph on the VLT [28]. It can observe wavelengths between 3000Å and 11000Å. The full spectrum is able to be observed, thanks to a dichroic that allows simultaneous measurement of the blue and red part of the spectrum. Only the red part of the spectrum of these stars has been analyzed by Nissan and Schuster (and others) already. However, the data describing the blue part of the spectrum has been ignored. The maximal resolution in the two arms of the instrument is respectively 80,000 and 110,000 for the blue and red part [28].

3.2 The sample

In the NS10 paper, three different groups of stars were identified by their kinematics. Firstly, the thick disk stars (TD), of the Milky Way. Secondly, the low-α halo stars, and lastly, there are the high-α halo stars. The halo stars clearly fall in two groups depending on the fraction of α elements.

To study the differences between the groups in NS10, two stars of each group are studied in this thesis. The name of the stars, as well as their group, Signal-to-noise ratio and UVES spectral resolution are given in Table 1.

Table 1: The resolution and Signal to noise ratio of the star sample

Star	Class	Resolution	S/N	Observation date	Program ID
HD148816	high-α	70000	260	2004-03-25	072.B-0179
HD76932	TD	70000	240	2004-03-30	072.B-0179
HD193901	low-α	70000	135	2004-03-27	072.B-0179
HD97320	TD	50000	115	2001-03-06	076.D-0086
CD-51 4628	low-α	50000	115	2001-03-08	076.D-0086
G18-39	high-α	50000	70	2015-06-26	095.D-0504

The spectral resolutions and S/N ratios for these stars are all rather high, especially for HD148816 and HD76932. This is required to hope to measure the weak spectral lines that heavy elements produce.

3.3 Radial velocity corrections

Upon gaining the spectra from ESO, some corrections had to be made. Firstly, I had to correct for radial velocity. The stars in the sample are either moving away from us or moving towards us, resulting in the spectrum being redshifted or blueshifted. This effect is dependent on the velocity in the following way:

$$\lambda_{observed} = \lambda_{rest}(\frac{v_{rad}}{c} + 1) \tag{5}$$

Where v_{rad} is the radial velocity of the observed star. To correct for this effect, we can use the following equation to obtain the original spectrum.

$$\lambda_{rest} = \frac{\lambda_{observed}}{\frac{v_{rad}}{c} + 1} \tag{6}$$

However, the radial velocity of the star is not the only movement that induces a shift in wavelength. The Earth is also moving around the Sun, which can either increase or decrease the apparent radial velocity of the star with up to 30km/s. This number is dependent on the date of the measurement and the location of the star in the sky. I took the simplest approach and used a few clear known iron lines, and shifted the spectrum until the iron lines were at the correct wavelength. The resulting velocity corrections, as well as the relative velocity compared to the sun, of the stars in the sample are displayed in Table 2.

Table 2: The radial velocities and measured velocities for the sample, as well as the difference between my measurement and that of Nissen and Schuster [12]

ID	Class	Measured velocity $\mathrm{km\,s^{-1}}$	Radial velocity [12] $\mathrm{km\,s^{-1}}$	Heliocentric correction [28] $\mathrm{km\,s^{-1}}$	Difference $\mathrm{km\,s^{-1}}$
HD148816	high-α	−71.0	−47.8	23.55	0.4
HD76932	TD	137.0	119.9	−18.68	−1.6
HD193901	low-α	−198.6	−171.2	26.91	−0.5
HD97320	TD	41.8	53.5	11.41	−0.3
CD-51 4628	low-α	192.5	197.9	5.98	0.6
G18-39	high-α	−260.0	−234.1	25.65	−0.3

Figure 8 shows the result of the velocity correction. Note that the two large iron lines within the figure are now at the right wavelength for all stars in the sample.

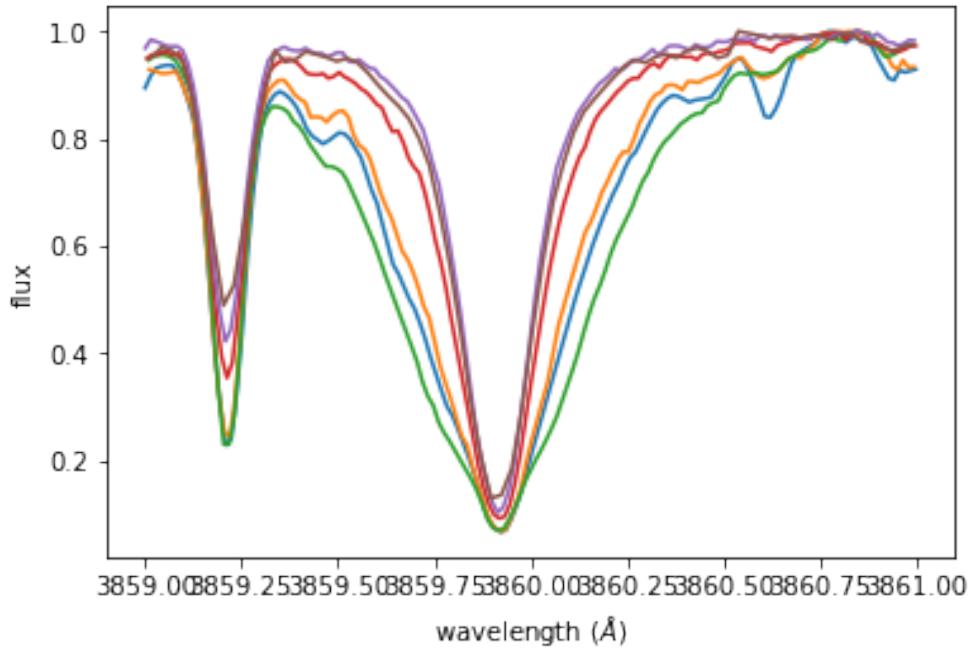

Figure 8: The spectra of all 6 stars in the sample, corrected for radial velocity using the values in the table above, around the 3859Å uranium line. The flux of the stars is divided by the maximum within this range for each star for normalization.

3.4 Continuum correction using polynomial

After putting the spectrum at rest frame wavelength, another correction had to be made to the observed spectrum in order to analyze it accurately. The total flux of each star varies with wavelength in the form of a black body Planck spectrum to first approximation. Even when there are no spectral lines involved, the flux of the star will be higher for some wavelengths than for others. One expects the flux from a star to approximately follow a black body spectrum, which is described by the following distribution:

$$B_\lambda(\lambda, T) \sim \frac{1}{\lambda^5} \frac{1}{e^{\frac{1}{\lambda T}} - 1} \tag{7}$$

However, due to a number of issues including detector sensitivity, as well as the fact that stars are not perfect black bodies, the resulting spectrum will not necessary follow that distribution exactly.

The problem is that the synthetic spectra used to analyze the spectral lines do not follow a black body distribution dependent on wavelength. Instead, the flux is set to 1 on default and drops in case of a spectral line. Additionally, setting the continuum to 1 makes it much easier to accurately detect lines and measure their properties. Hence the black body-like shape should be removed from the observed spectrum, and afterwards, the continuum should be set to 1. This is called normalisation.
To do this, I first selected sections of the continuum where there were no spectral lines, as seen in Figure 9. At these points, I can assume the corrected spectrum would be 1.

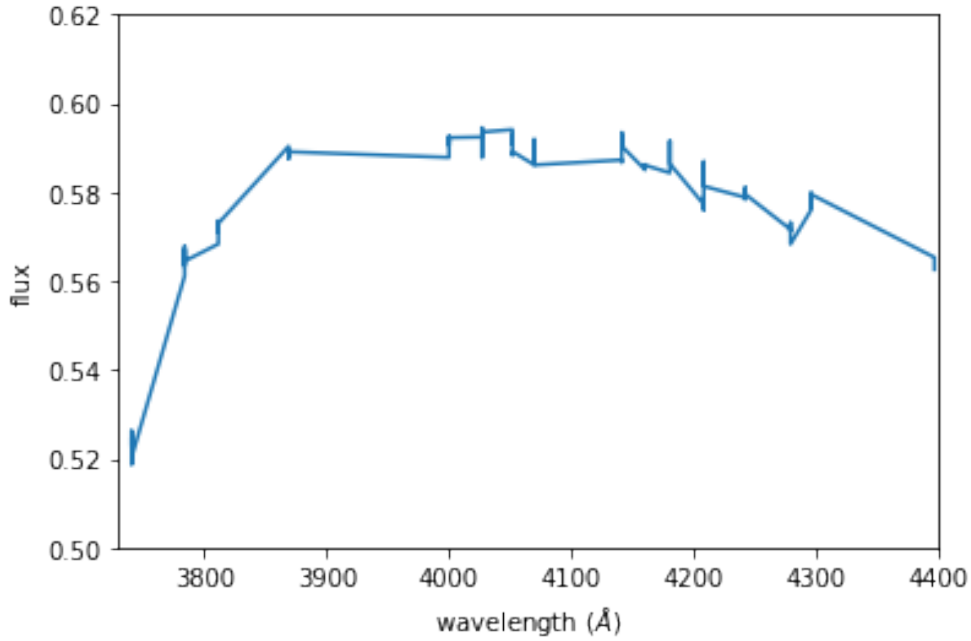

Figure 9: The flux in the selected sections of the spectrum of star CD-51 4628

Then, a polynomial was fitted through those sections. An example is shown in Figure 10.

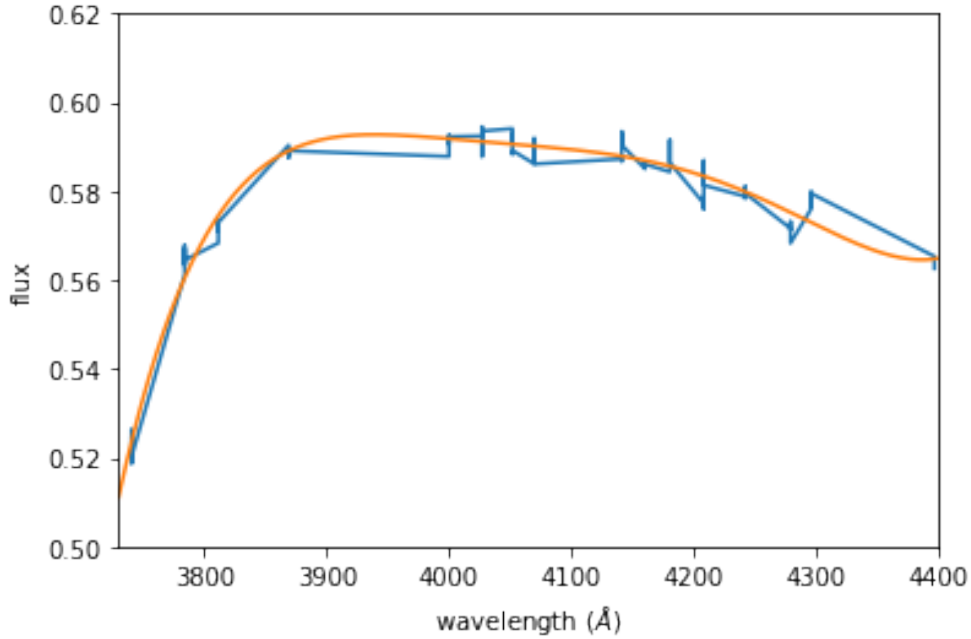

Figure 10: The fitted 5-th degree polynomial through the selected sections of the spectrum of star CD-51 4628

One thing to note here is that there are not many line free regions of the spectrum taken into consideration below 4000Å. This is in particular because of the many strong hydrogen and calcium lines in this part of the spectrum. Due to these lines, the flux within this region is almost always significantly lower than it would be without those lines, which makes it difficult to accurately evaluate the continuum at these wavelengths.

After creating the polynomial, the flux was divided by the polynomial to obtain the normalized flat spectrum of each star.

4 Abundances of interest

4.1 Choosing elements and lines

Once the corrected spectra were obtained, I had to choose the elements which I wanted to measure, and determine whether it was feasible to do that and which lines to use if it was. Even though we are most interested in the heavy r-process elements, it was also necessary to determine the abundances of some of the lighter elements.

Table 3: The solar abundances assumed for the individual elements during this thesis, in $\log(\epsilon)$ units, adopted from Solar Elemental Abundances [29]. Note that uranium has only been measured as an upper bound.

element	number	Abundance ($\log(\epsilon)$)
H	1	12.00
Mg	12	7.56
Ca	20	6.32
Fe	26	7.48
Sr	38	2.83
Ba	56	2.25
La	57	1.11
Eu	63	0.52
Th	90	0.03
U	92	-0.47*

4.1.1 Iron

Measuring the iron abundance is a necessity. The abundance of heavy elements is almost always compared to the iron abundance of said star, and just the iron abundance already gives a lot of information about said star. Additionally, the amount of iron lines is so large that it is highly likely for the lines of other elements to be at least partially blended with the iron lines. Fortunately, there is an overabundance of strong lines to choose from when measuring the iron abundance. Even after filtering out blended lines, I was still left with 25 useful iron lines to use in this thesis.

4.1.2 α elements magnesium & calcium

Two other light elements that had to be measured were magnesium and calcium. Both of these elements have enormous lines that affect a significant part of the spectrum. In case of calcium, both the 3933.6614 Å line and the 3968.4673 Å line depress the continuum for tens of Angstroms. In case of magnesium, the largest lines are a bit smaller, but the 3838.292 Å and the 3832.000 Å lines still depress a significant part of the local continuum. Another reason for measuring these two elements is that they were also both measured in NS10 as part of the alpha elements. magnesium was also the element used to make the distinction between the low-α and high-α groups, as can be seen from the striped line in Figure 5.

For magnesium and calcium, the amount of usable lines was significantly less than iron. However, for both of those elements, I ended up with 4 unblended lines.

4.1.3 Heavy elements

In this thesis, I am mostly focusing on the r-process elements, and especially the heavy ones. Therefore, when choosing the elements from which the abundances would be measured, I first looked at the heaviest observable r-process elements. These are uranium and thorium.

To check whether measuring these rare and heavy elements was even possible, I created a synthetic spectrum for the stars in my sample where I assumed that the uranium and thorium abundance was equal to 0 in $\log(\epsilon)$ units. This is approximately equivalent to the amount of these elements in the sun in the case of thorium, and significantly higher in the case of uranium. Additionally, a synthetic spectrum was created with practically no thorium or uranium at all, setting the abundances at -9.99 in $\log(\epsilon)$ units. In the chapter 5 of this thesis, the method of obtaining the synthetic spectra is described.

Now, I compare these two synthetic spectra and the real spectrum at the strongest thorium and uranium lines. If the two synthetic spectra are practically equivalent at these lines, one can already conclude that the spectral lines are not sensitive to this element. However, if the two synthetic spectra are different, and the real spectrum

looks somewhat like the synthetic spectrum with a non-zero abundance of the element, it is an indication that one is able to measure the abundance of these elements. In the case of uranium, there is unfortunately almost no difference between the two synthetic spectra, as can be seen in Figure 11 below, which depicts the strongest line at $\lambda = 3859.5716$Å. Even though it is the best uranium line, it still has only been measured in a handful of stars, one of which is the metal poor giant CS 31082-001 [23]. Other complications for measuring that element include the best line being within the outskirts of a strong iron line and the synthetic spectrum having trouble modelling the region accurately enough to measure a weak and blended line.

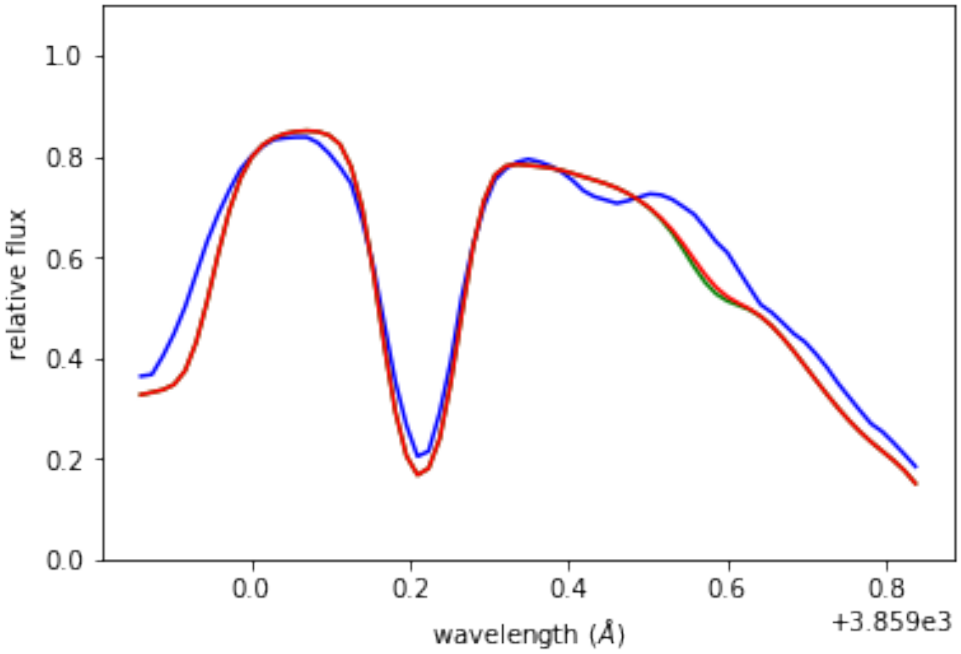

Figure 11: The 3859 Å uranium line for star HD148816 (blue). The synthetic spectra have an abundance of 0 (log ϵ, green) and -9.99 (log ϵ, red)

In case of thorium, there is a promising line, at $\lambda = 4019.1289$Å, that is most often used in literature. Examples include the paper by A.P. Ji and A. Friebel [22], the paper by R. Cayrel et al [23], and the paper by A. Yushchenko et al [25]. In Figure 12 below, said line is shown for star HD76932

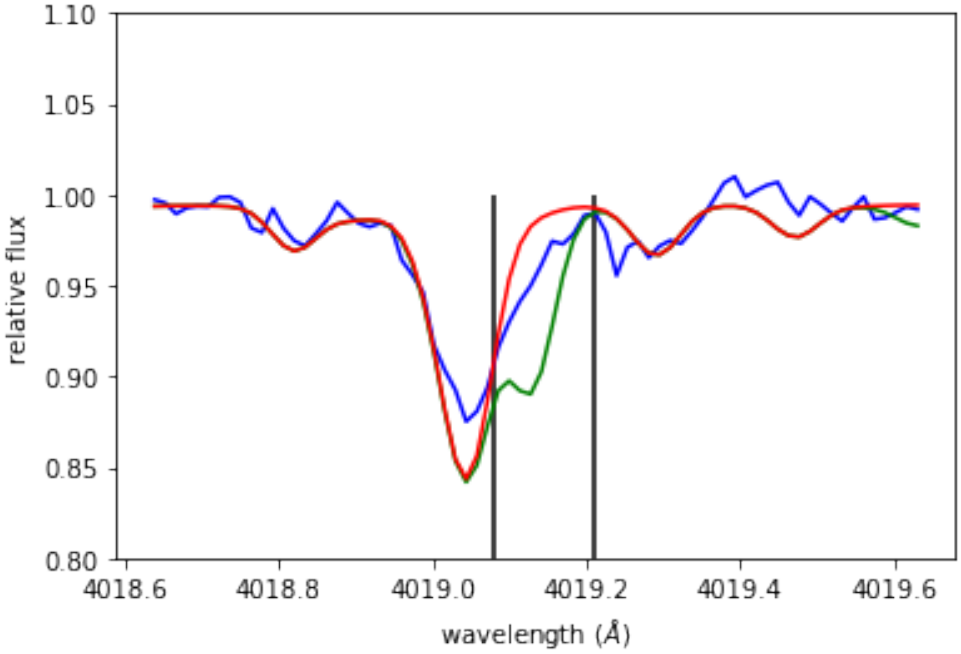

Figure 12: The thorium 4019Å line for the thick disk star HD76932 (blue). The synthetic spectra have an abundance of 0 (log ϵ, green) and -9.99 (log ϵ, red)

In Figure 12, we see clearly that the observed spectrum is depressed at the 4019.1289Å thorium line. Hence,this is a likely detection of thorium, and an abundance can be obtained. Most other stars in my sample also show similar clear depressions in the spectrum at the location of the thorium line. Unfortunately, other thorium lines, like the 4116.7137Å and the 4381.8616Å line shown in Figures 13 and 14, seem too weak or too blended to be useful.

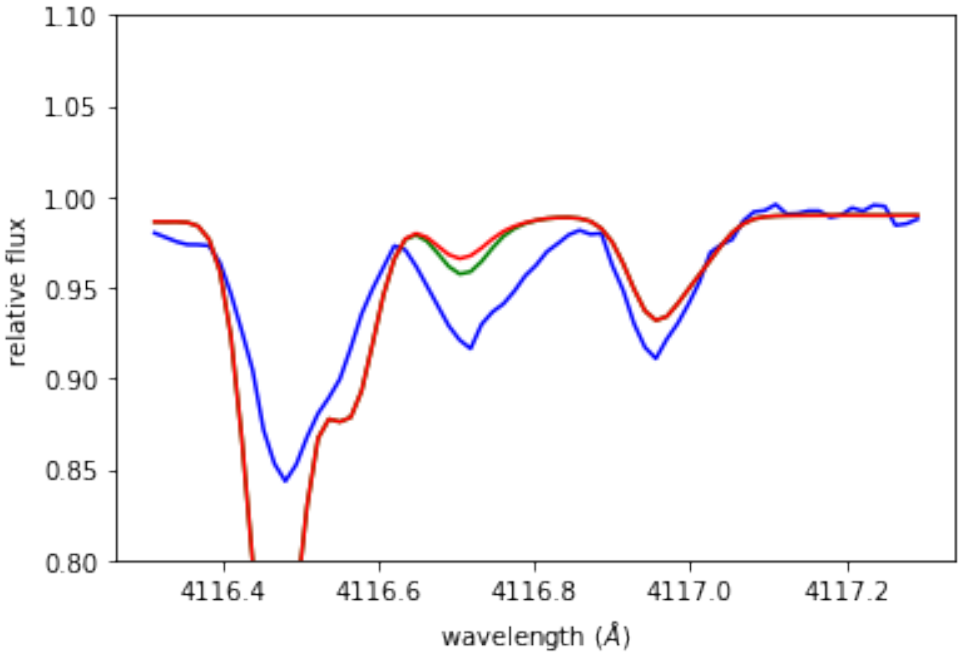

Figure 13: The thorium 4116Å line for star HD148816 (blue). The synthetic spectra have an abundance of 0 (log ϵ, green) and -9.99 (log ϵ, red)

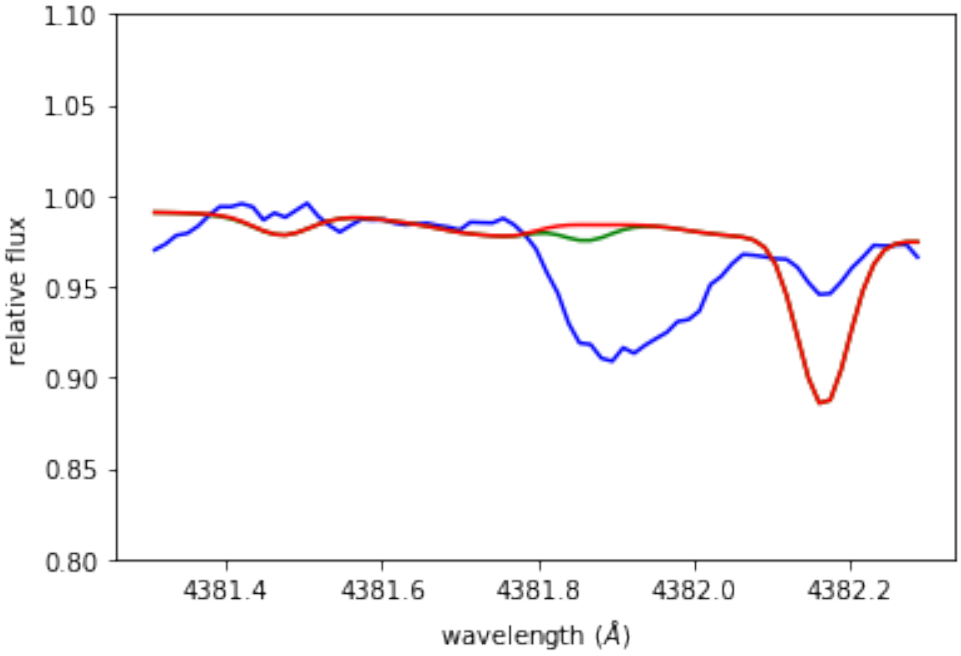

Figure 14: The thorium 4381Å line for star HD148816. The synthetic spectra have an abundance of 0 (log ϵ, green) and -9.99 (log ϵ, red)

Additionally, europium is measured as it is a pure r-process element and has a strong lines that are easily measurable. Because of that, it is often used in literature. It also has a very strong spectral line within the wavelength range without any significant blending with other spectral lines.

Unfortunately, it is hard to measure other heavy r-process elements. platinum, a 3-rd waiting point r-process

element, does not have any strong lines within our range of wavelengths. The strongest lines are instead at 3408.13Å, 3064.71Å and 2929.79Å, significantly lower than the minimum wavelength of 3730Å of our observed spectrum. rhenium and gold have similar issues, with no reasonably strong lines within our wavelength range. Iridium and osmium do have some lines within our wavelength range. However, these are rather weak lines and would not give reliable results. If lower wavelengths had been observed, then those r-process elements abundances could have been measured, like J.J. Cowan et al [30] did for platinum and osmium using the 2600-3100Å wavelength range.

Even though it is not the main focus of this thesis, it is still useful to measure s-process elements. Therefore barium and strontium, two almost pure s-process elements with strong lines in our wavelength range are also measured. Additionally, lanthanum, which is possibly an indicator of the not yet confirmed i-process, has multiple strong lines within the wavelength range and will also be measured.

5 Synthetic Spectra

To use the absorption lines in the stellar spectra to determine abundances, we need to make a model. These models are called synthetic spectra.

5.1 Turbospec

To create the synthetic spectra, the Turbospec program was used [31]. This program generates stellar spectra using an atmospheric model for each star, using as input physical parameters: T_{eff} and log g. Here we adopted the stellar, atomsperic parameters from NS10. The atmospheric model was created using MARCS models [32], which will be discussed in the next subsection. The basic parameters are assumed to be the same as in the Nissan and Schuster paper, and are shown in Table 4.

Table 4: The basic parameters of the target stars, adopted from Nissen and Schuster [12]

ID	Class	T_{eff}	log g	turbulent velocity (km s^{-1})
HD148816	high-α	5823	4.13	1.4
HD76932	TD	5877	4.13	1.4
HD193901	low-α	5656	4.36	1.3
HD97320	TD	6008	4.19	1.6
CD-51 4628	low-α	6153	4.31	1.4
G18-39	high-α	6040	4.21	1.5

5.2 MARCS

To create the atmospheric models used in Turbospec, we first needed to download a grid of MARCS model atmospheres [32] with stellar parameters similar to the star in question. Then, as none of the provided model atmospheres would have the exact same stellar parameters as the star of interest, the final model atmosphere was interpolated using the provided program from the grid of model atmospheres.

5.3 Correcting resolution

After obtaining a synthetic spectrum, it cannot be directly compared with the real spectrum. This is because the synthetic spectrum is generated with extremely high spectral resolution. We have to deconvole this spectrum to the observed spectral resolution. This involves rebinding the pixels to match the observed spectral resolution, as given in Table 1. I used the code provided by D. Sardjan to do the deconvolution. After the spectrum is deconvolved, linear interpolation is used to match the wavelengths of the individual points of the synthetic spectrum to those of the real spectrum.

5.4 Grid creation

To find the abundance values of the element of interest, one first has to create a large grid of synthetic spectra where the abundance of the element of interest is different for each individual spectrum. For example, in the case of strontium, the grid of possible Sr abundances stretches from 0.50 and 2.50 in $\log(\epsilon)$ units, with steps of 0.05. Additionally, a spectrum with an abundance of -9.99 in $\log(\epsilon)$ units is created to identify possible blending with other nearby lines. If the synthetic spectrum with negligible Sr abundance is still depressed, then there is another

nearby line that affects the real spectrum at this wavelength. In that case, it is usually best to use another line if available. An plot with multiple synthetic spectra of Sr is shown in Figure 15 to visualize the grid method.

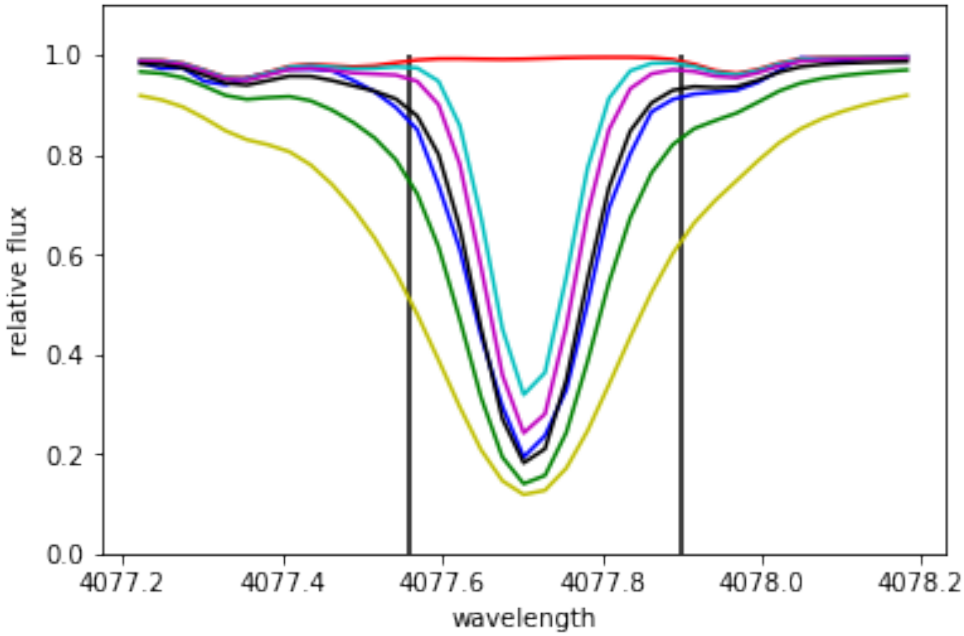

Figure 15: The best strontium line of star G18-39 simulated using synthetic spectra with different values for strontium, varying from 0.5 (cyan) to 2.5 (yellow) (in log ϵ units) with steps of 0.5. The dark blue line corresponds to the real spectrum, while the red line corresponds to the synthetic spectrum with a negligible strontium abundance of -9.99 (log ϵ).

Once all the different spectra of the lines of interest are created using Turbospec, they are compared with the original spectrum using a chi-square fitting method. For this, one first needs to find the line or lines of interest, and then define a region around said line of interest where the synthetic spectrum should be compared to the real spectrum. Note that if part of the line is likely blended with another line, which can be checked by using the synthetic spectrum with negligible abundance, then it is best to only use the part of the line where blending is not an issue. An example of this is shown in Figure 15, where the wings are not taking in consideration because of lines at 4077.5 and 4078.0 Å.

6 Obtaining abundances

Before measuring the heavy chemical elements of interest, we first needed to find the abundances of the more common elements in order to make the synthetic spectrum more accurate. The iron abundance was especially important because some lines of interest are within the outskirts of deep iron lines. Therefore, I first obtained the iron, calcium and magnesium abundances before analysing the heavy elements.

6.1 Chi-square fit

When the region around the line of interest is defined, and the grid of synthetic spectra with different abundances is generated, then one can use the Chi-square fitting method to determine the most likely abundance of the element of interest. Each individual synthetic spectrum will be fitted against the real spectrum, and the chi-square value of said fit within the region of interest is calculated. Once all chi-square values are obtained, one can find the most likely abundance by finding the minimal chi-square value and taking the corresponding abundance. A plot of the chi-square value against the abundances can also be used to verify this.

For the weak lined heavier elements, the grid of synthetic spectra had rather large steps of 0.05, while for the strong lined lighter elements, the grid had steps of only 0.02, and the true minimum of the chi-square plot has therefore an uncertainty of ± 0.025. To get a more accurate result, the chi-square plot was interpolated using a second degree polynomial. With this method, the step size was artificially decreased to 0.01. The main advantage of this is that it is now possible to get results up to two decimal point. However, the interpolation might be a bit off from the real values, so abundance uncertainty from the fit is still ± 0.01.

6.2 Confidence interval for a single line

There are multiple sources of uncertainty. First, there is the uncertainty in the exact minimum of the chi-square graph, which is ± 0.01 at best. Secondly, and more importantly, there is the uncertainty in abundance measurement. This uncertainty exists because it is not much less plausible that a synthetic spectra with a slightly worse fit is the true abundance. Therefore, any synthetic spectra with a chi-square value for the fit that isn't much higher than the minimum could correspond to the real abundance level. Sources of the uncertainty in finding the optimal abundance include errors in continuum evaluation and random noise in the spectrum. This uncertainty is rather hard to measure, and there are two methods of estimating it.

The first method is to estimate confidence intervals by hand, using the visible variation in the real spectrum. The main advantages of this method are that it is simple and can always be done to reasonable approximation, even if the real spectrum is unusual. However, this method has the disadvantage of being slow and a lot of work. Additionally, it is very hard to do it consistently and unbiased, as it is done by a human instead of by a program.

The second method, and the method I use, is to first determine a χ^2 range, and every abundance in this range is within the confidence interval. The main advantages of this method are that it is very fast and doesn't take a lot of work once the χ^2 range is determined. Additionally, the method is unbiased and consistent. However, there are some disadvantages to this method. It is very important to determine the range accurately, because otherwise the confidence intervals will be consistently too small or too large. Additionally, this method can have some issues if a certain synthetic spectrum at a very weak line appears to fit the real spectrum too well, but the difference in models is very small. In Figure 16, an example for such a situation is shown.

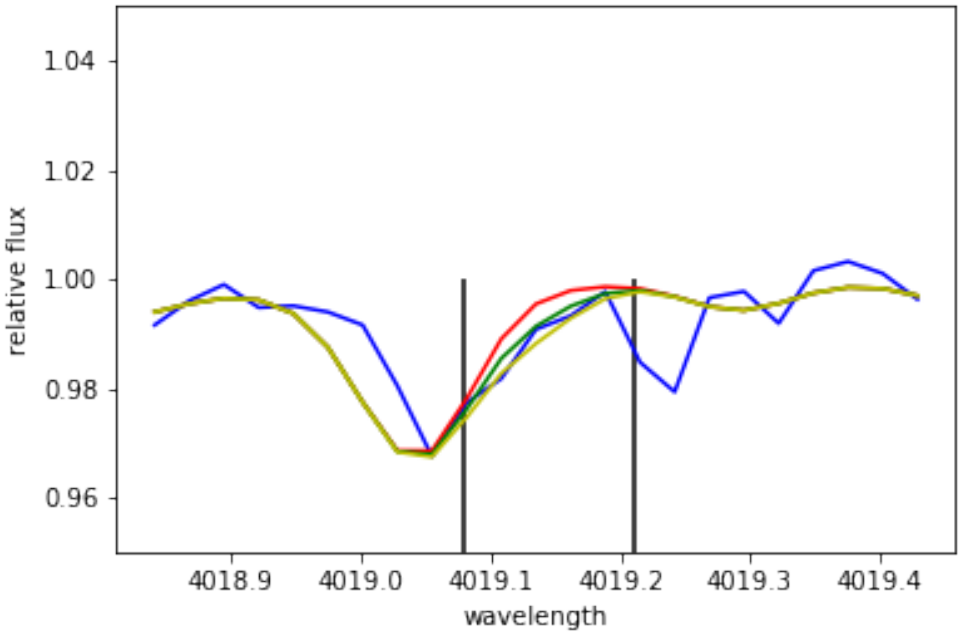

Figure 16: The confidence interval generated for the thorium line of star G18-39 using the chi-square method. The green and yellow lines are the upper and lower limits for the automatically generated confidence intervals, the blue line corresponds to the real spectrum, and the red line to a synthetic spectrum with negligible Throium (-9.99 $\log(\epsilon)$).

One can immediately spot in Figure 16 that the confidence interval is much too small, especially compared to the variation in the real spectrum, and this causes an extremely low minimum chi-square value. In Figure 17 one can see that the minimum comes extremely close to 0.

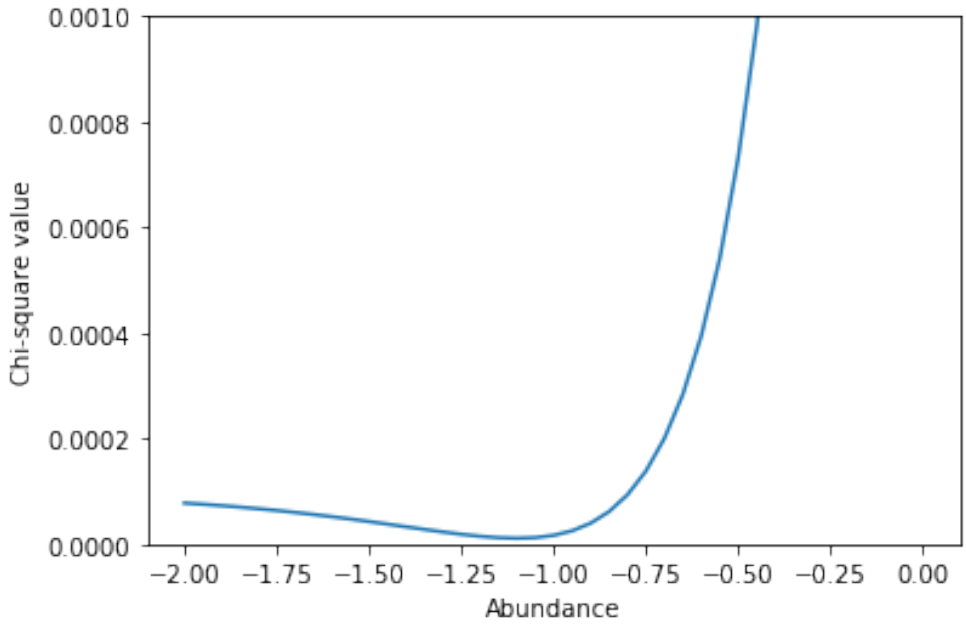

Figure 17: The chi-square fit for the thorium line of star G18-39 as shown in Figure 16 for a grid of different abundance values of thorium.

The solution for this is to inspect confidence intervals that seem suspiciously small. If they are indeed found to be too small, then the confidence intervals should be determined manually for these lines. For the above example, the manually generated confidence intervals are shown in Figure 18.

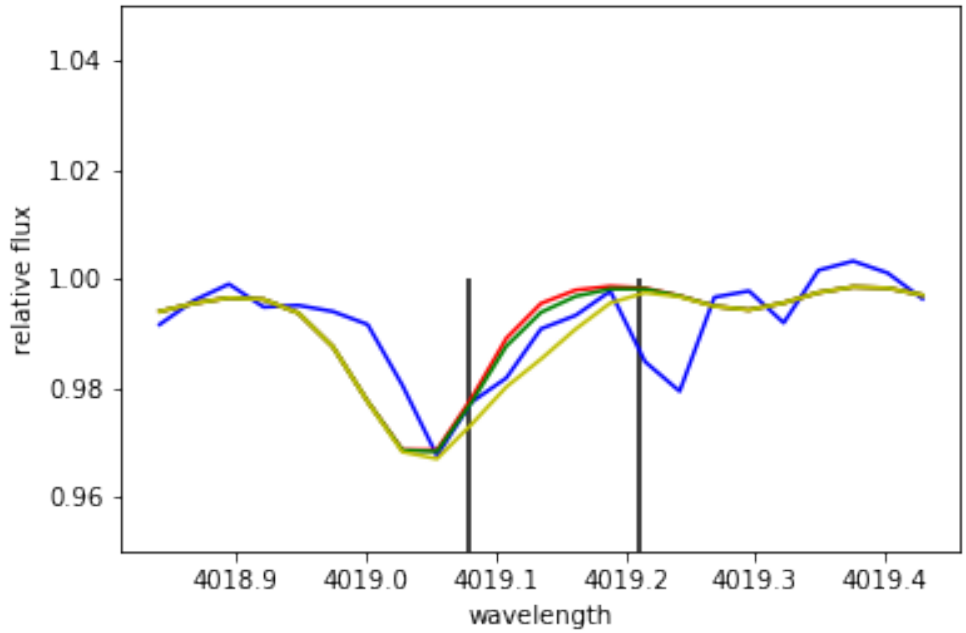

Figure 18: The improved confidence interval determined visually for the thorium line of star G18-39. The green and yellow lines are the upper and lower limits for the automatically new confidence intervals, while the blue line is the real spectrum.

The suitable χ^2 range was determined using the lanthanum lines. For all these 4 lines, the optimal abundance was estimated. Then, using these 4 estimates, the standard deviation was estimated. As the confidence interval should be approximately 2 times the standard deviation on both sides, I used that for an estimation of the size of the confidence interval of a single line.

6.3 Multiple lines

In case of multiple lines, the abundances are determined somewhat differently. The chi-square method is still used. However, the abundance is now taken as the mean of all individual abundances. The confidence interval is now also calculated differently. In this case, it is calculated as the error of the mean, which can we calculated as follows.

$$\sigma_{mean} = \frac{\sigma}{\sqrt{N-1}} \tag{8}$$

where σ is the standard deviation for the abundances of the sample of lines, and N the number of lines.

Here, we show how the optimal iron abundances were calculated using the chi-square method for 25 individual iron lines. We show an example in Figure 19 for star HD148816 and in Figure 20 for star HD76932.

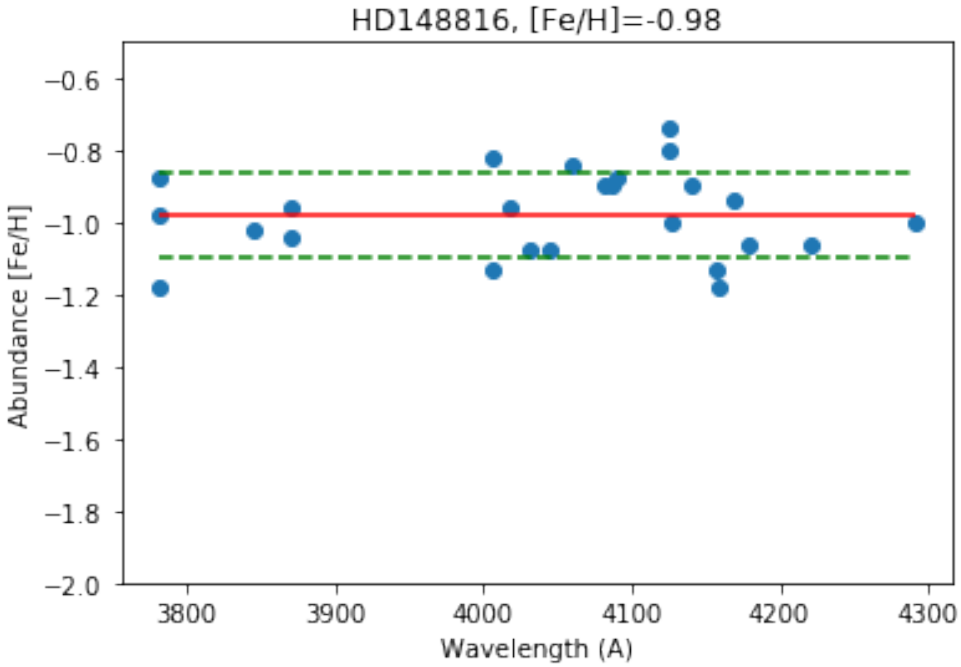

Figure 19: The obtained iron abundances from all 25 different lines in star HD148816. The mean (red) and standard deviations (green dashed) are shown and the mean value is [Fe/H]= -0.98 ± 0.12

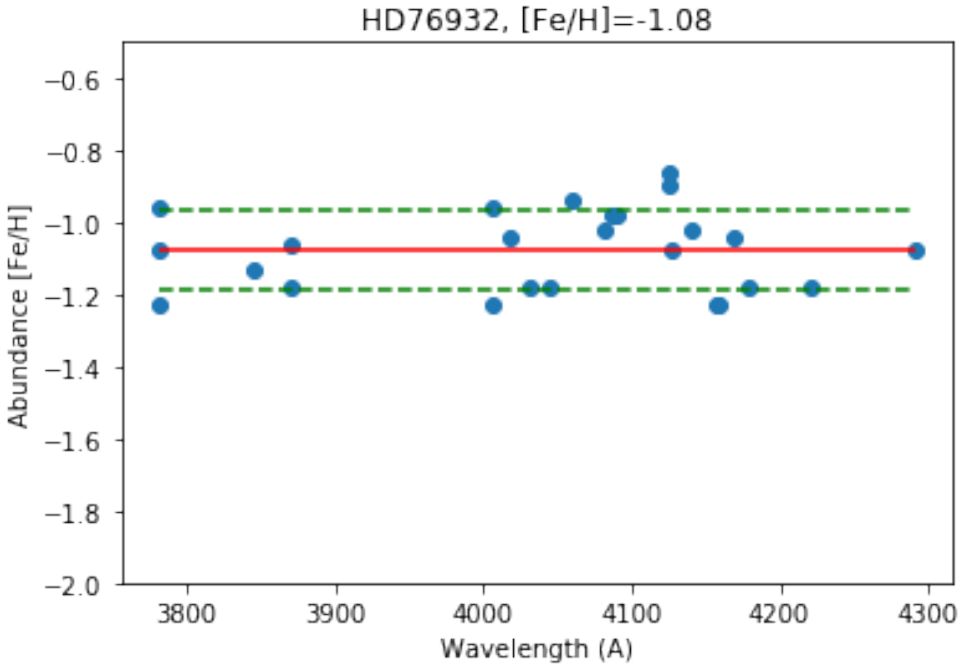

Figure 20: The obtained iron abundances from all 25 different lines in star HD76932. The mean (red) and standard deviations (green dashed) are shown and the mean value is [Fe/H]= -1.08 ± 0.11

One thing that is striking from these figures is that some lines always seem to overestimate the iron abundance, while other lines seem to always underestimate the abundance. Additionally, this seems to be uncorrelated with the wavelength. This could be due to errors in the synthetic spectra or uncertainties in our understanding of the lines.

What we saw with the iron lines if far more striking with the magnesium lines. Within the wavelength range, there are only a few magnesium lines that are suitable without much blending with other lines. Out of the 4 best lines, two always seem to overestimate, and the other two always seem to underestimate the magnesium abundance. This leads to extremely large uncertainty intervals in the magnesium abundance, making their size comparable to the uncertainty intervals for europium. Two examples are given in Figures 21 and 22.

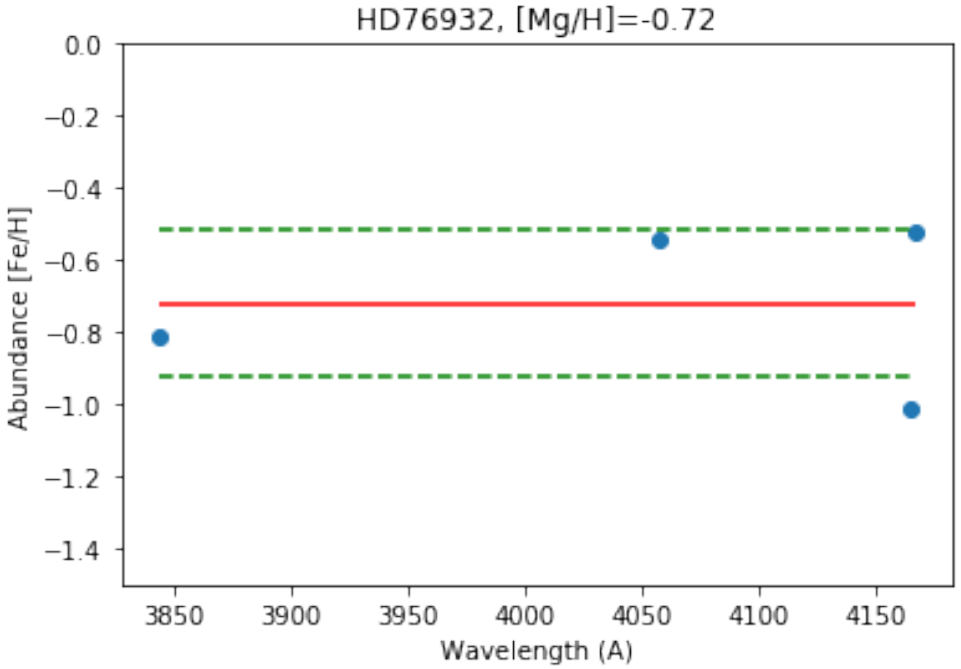

Figure 21: The obtained magnesium abundances from all 4 different lines in star HD76932. The mean (red) and standard deviations (green dashed) are shown and the mean value is [Mg/H]= -0.72 ± 0.20

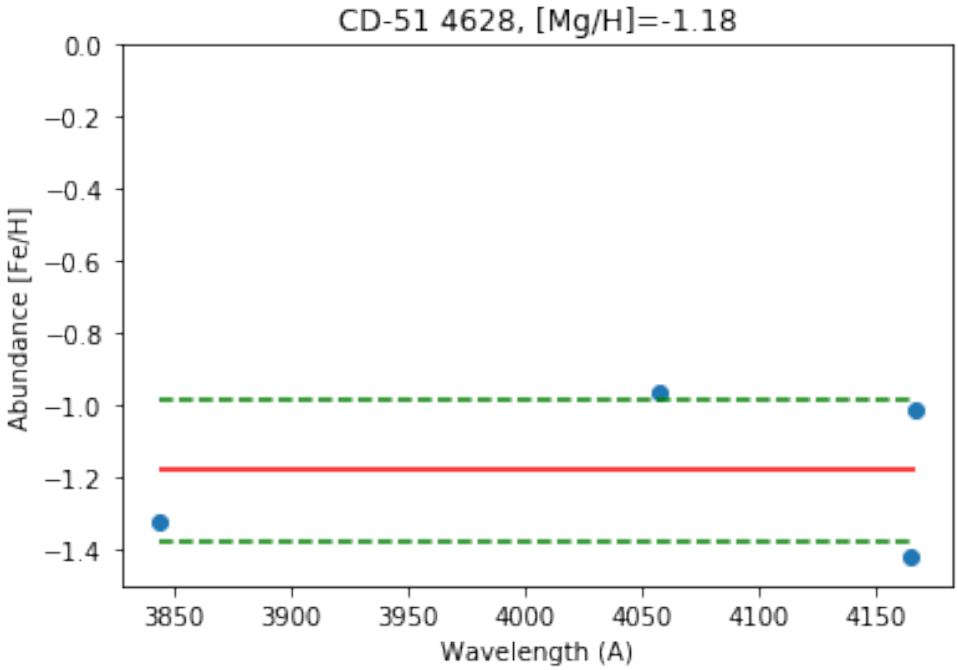

Figure 22: The obtained magnesium abundances from all 4 different lines in star CD-51 4628. The mean (red) and standard deviations (green dashed) are shown and the mean value is [Mg/H]= $-1.18\pm$ 0.20

For most of the analysis, the absolute values of the magnesium abundance do not matter. Instead, we are more interested in the relative values of the stars compared to eachother. Therefore, we can observe the abundance of a strong individual biased line with its assorted smaller confidence interval and use that for part of our analysis.

7 Results

Using the methods described in the previous sections, the abundance of all elements of interest was measured in the star sample. In table 5, all observed abundances are given.

Table 5: Abundance ratios for the sample of stars

ID	Class	$[\frac{Fe}{H}]$	$[\frac{Ca}{Fe}]$	$[\frac{Mg}{Fe}]$	$[\frac{Sr}{Fe}]$	$[\frac{Ba}{Fe}]$	$[\frac{Eu}{Fe}]$	$[\frac{La}{Fe}]$	$[\frac{Th}{Fe}]$
HD148816	high-α	-0.98	0.25	0.35	0.16	-0.16	0.34	0.16	0.64
HD76932	TD	-1.08	0.28	0.36	0.30	-0.03	0.45	0.31	0.64
HD193901	low-α	-1.29	0.20	0.19	-0.07	-0.03	0.49	0.26	0.62
HD97320	TD	-1.33	0.27	0.37	0.16	-0.17	0.27	0.24	0.34
CD-51 4628	low-α	-1.45	0.20	0.27	0.12	-0.13	0.52	0.33	0.48
G18-39	high-α	-1.65	0.30	0.55	0.45	0.14	0.46	0.41	0.52

The first thing to note from this table is that a non-zero abundance was found for all elements. This is especially striking for thorium, which is rarely observed in literature. Another thing we observe from the table is that the r-process elements and lanthanum have abundances higher than solar for all stars, while barium and strontium abundances are close to solar for those stars. For more detailed interpretation, we will make use of figures.

7.1 Lighter elements

The first element measured in this analysis was iron. As Nissen and Schuster also measured the metalicity of the stars in the sample, I could compare my results, displayed in Table 5, with them. In Figure 23, the difference between our observations is plotted against the metalicity measured in this thesis.

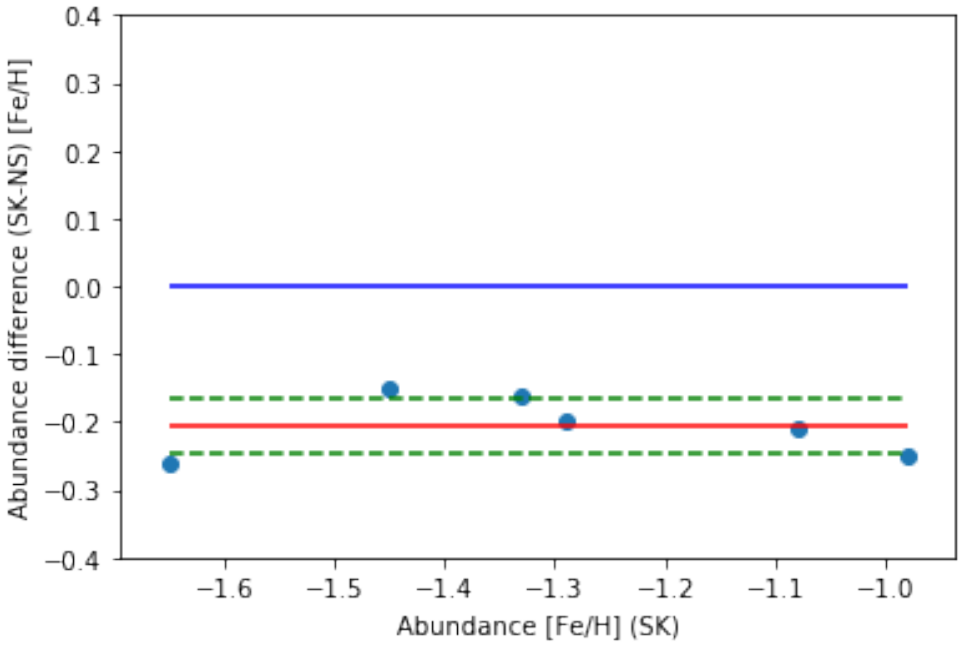

Figure 23: The difference in measured metalicity between me (SK) and the Nissen and Schuster paper (NS) [12] for the 6 stars in the sample plotted against the metalicity measured in my thesis. The red line denotes the mean difference and the green striped lines the standard deviation

From Figure 23, it is clear that my measurements for the metalicity are lower than those done by Nissen and Schuster. However, the difference is consistent for all stars, being approximately 0.21 for all of them. Hence, this points towards there being a systematic offset in the metalicity scale with Nissen and Schuster. However, if the bias is similar for all other measured elements, then there should be no issue for the analysis because all other abundances will be given in $[x/Fe]$ units, which will cancel out any systematic bias.

The second measured element was calcium. In Figure 24, the Ca abundances are plotted against the metalicity for both my thesis and the Nissen and Schuster paper.

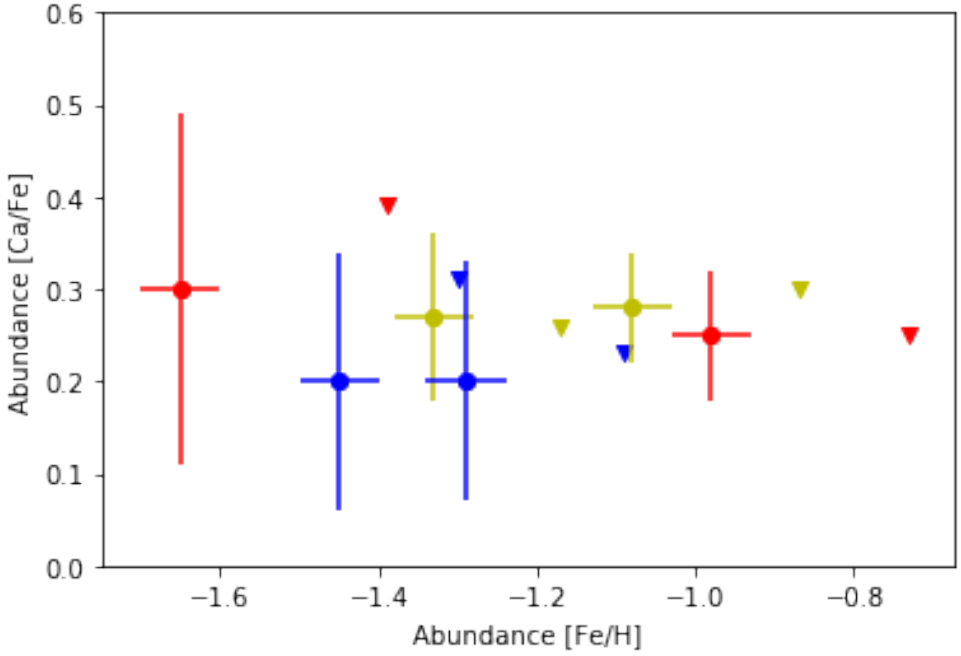

Figure 24: The calcium abundance from my analysis (circles) with their 95% confidence intervals, and from the NS paper (triangles). Blue are low-α, red are high-α and yellow TD.

From Figure 24, one has to note that my iron abundances are lower than those of Nissen and Schuster, leading to a shift to the left in the figure between the results from Nissen and Schuster and my own. After accounting for

that, we observe that my measured calcium abundances are either similar or slightly lower than those measured by Nissen and Schuster. As the differences are much smaller than the 0.21 difference in iron abundance, it confirms that the bias in calcium abundance is similar to that in the iron abundance, leading to them canceling each other out in $[Ca/Fe]$. Secondly, analysis finds the same low-*alpha* and high-α distinction within the sample as NS10, albeit at slightly different levels.

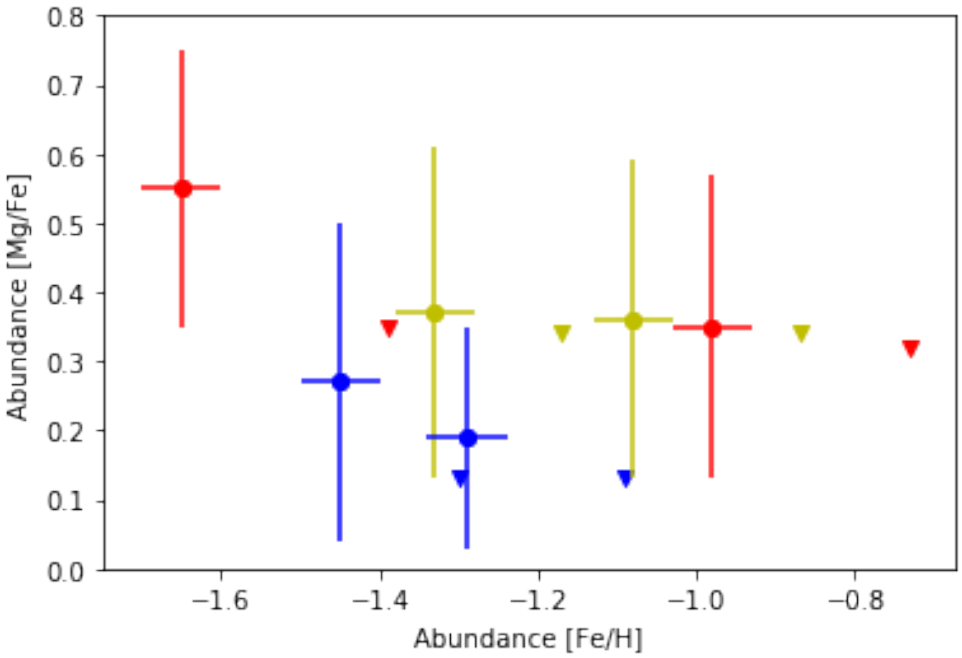

Figure 25: The magnesium abundance from my analysis (circles) with their 95% confidence intervals, and from the NS paper (triangles). Blue are low-α, red are high-α and yellow TD.

In Figure 25, my observed magnesium abundances are compared to those from NS10 in the same way as in the calcium plot. In this case, it is clearly visible that my observations and those of NS10 varying between the stars. Star G18-39 is especially notable for having a much higher magnesium abundance in my observations than in those from NS10. This is almost certainly a direct consequence of the large discrepancy in the abundances from the individual magnesium lines and the large uncertainty intervals that resulted from that. However, it is still clearly visible that the magnesium abundances are lower for the low-α stars when compared to the high-α stars, leading to the same conclusion as in the NS10 paper.

7.2 Heavy elements

In figures 26 to 30, the abundances of the heavy elements, given in table 5, are plotted against the iron abundance for the heavier elements. Additionally, their 95% confidence (2σ) intervals are shown.

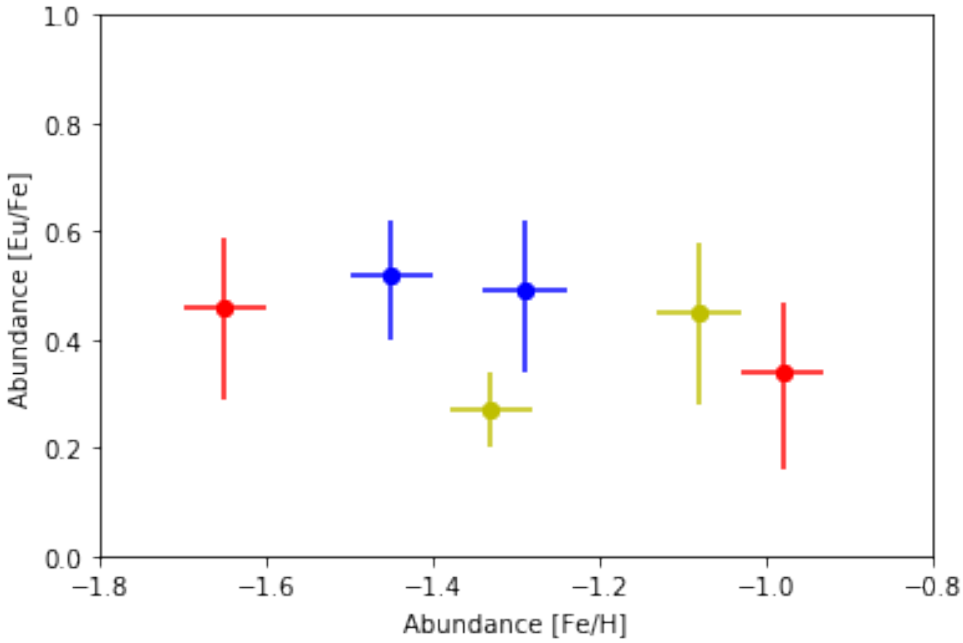

Figure 26: The europium abundance for my stellar sample. Blue are low-α, red are high-α and yellow TD.

From Figure 26, we observe that there is not much variation between the europium abundance of the different stars. The Low-α stars on average have a slightly higher abundance, but that difference is not significant.

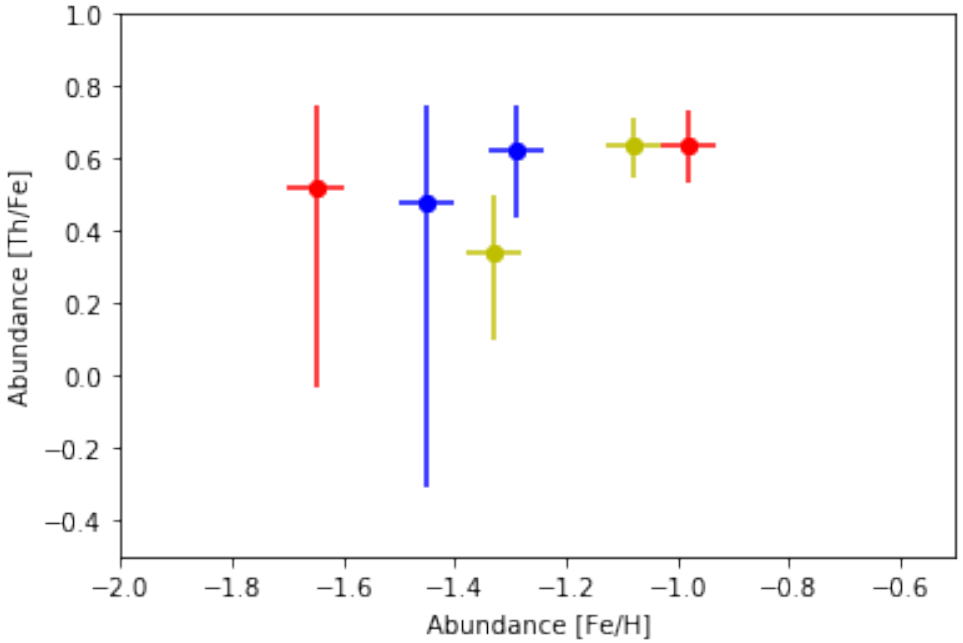

Figure 27: The thorium abundance for my stellar sample. Blue are low-α, red are high-α and yellow TD.

From Figure 27, the first striking observation is the enormous confidence intervals of the two most metal-poor stars, which limits the conclusions we can draw from them. The other 4 stars have very similar thorium abundances, although the abundance of HD97320 is a bit lower.

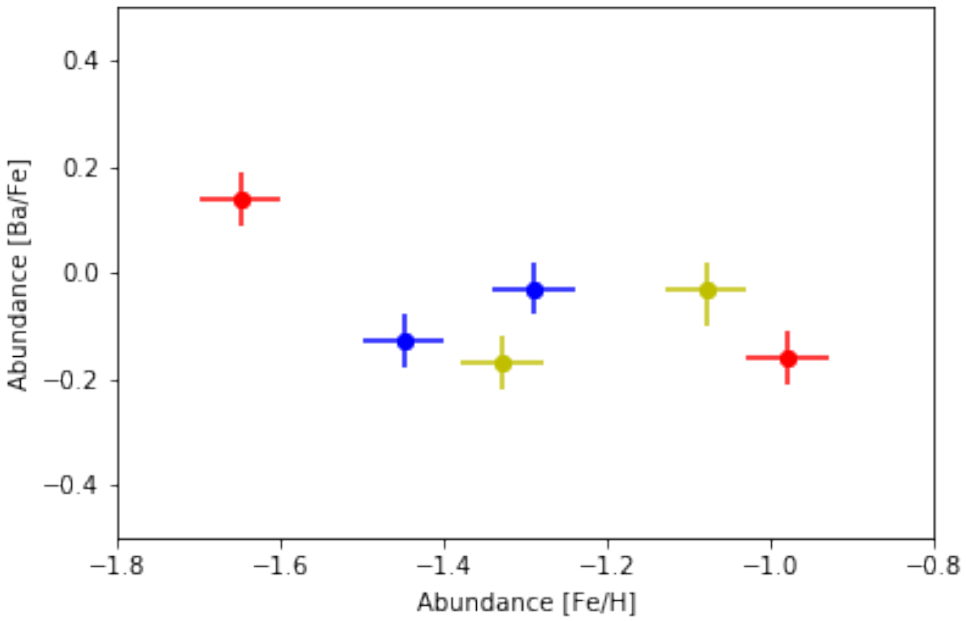

Figure 28: The barium abundance for my stellar sample. Blue are low-α, red are high-α and yellow TD.

The most striking part of Figure 28 are the small confidence intervals, even though there is only one barium line measured. This is because the one barium line that is measured is a strong line with almost no blending, resulting in accurate measurements. With a single exception, all barium abundances are similar at slightly below solar. The exception is star G18-39, which has a barium abundance slightly above solar.

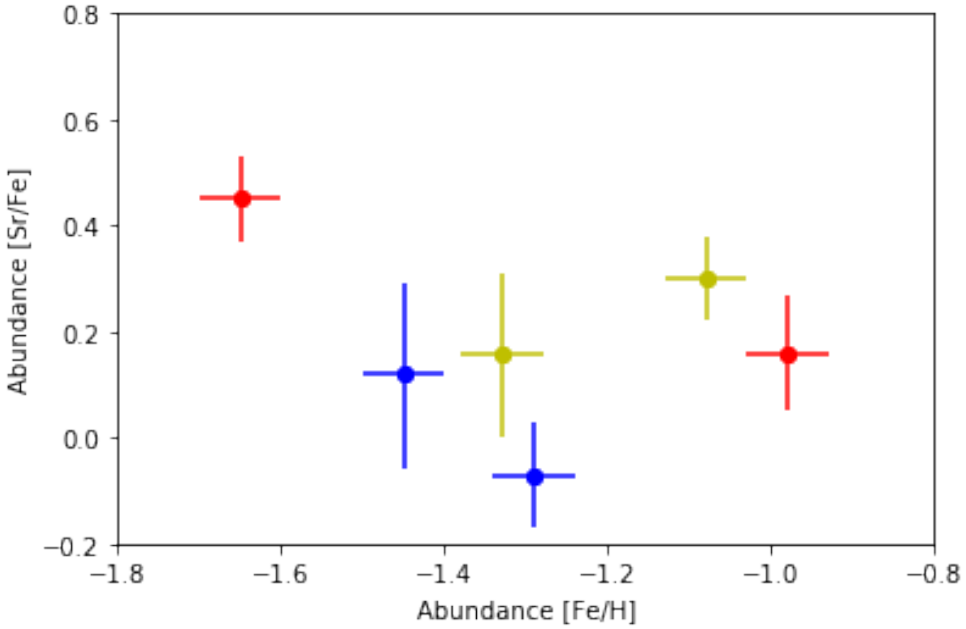

Figure 29: The strontium abundance for my stellar sample. Blue are low-α, red are high-α and yellow TD.

For strontium, we see in Figure 29 that the error bars are slightly larger than those of barium, although not too big to draw conclusions. Again, we see that star G18-39 has an abundance higher than the other stars. As this was also the case for barium, this is an indication that said star has more s-process elements in general. The other stars have similar abundances in general, although those the low-α stars seem to be slightly lower.

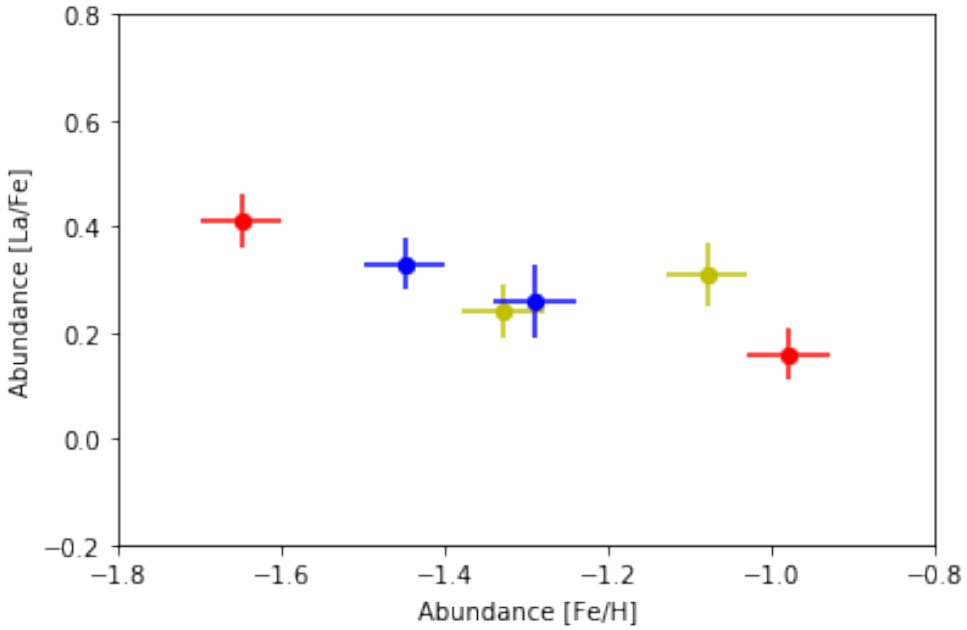

Figure 30: The lanthanum abundance for my star sample. Blue are low-α, red are high-α and yellow TD.

Like barium, the confidence intervals for lanthanum shown in Figure 30 are very small. In this case, there are 4 strong lines without much blending. Additionally, unlike for magnesium, the optimal abundances of those lines are in good agreement with each other. There is not much variation in between the stars. Like in the case of the pure s-process elements, G18-39 has the highest abundance, but the difference is not as striking as for Ba.

Table 6: Heavy element abundance ratios for the sample of stars

ID	Class	$[\frac{Fe}{H}]$	$[\frac{Th}{Eu}]$	$[\frac{Eu}{Ba}]$	$[\frac{Sr}{Ba}]$	$[\frac{Sr}{Eu}]$	$[\frac{La}{Ba}]$	$[\frac{La}{Eu}]$	$[\frac{Eu}{Mg}]$
HD148816	high-α	−0.98	0.30	0.50	0.32	−0.18	0.32	−0.18	−0.01
HD76932	TD	−1.08	0.19	0.48	0.33	−0.15	0.34	−0.14	0.09
HD193901	low-α	−1.29	0.13	0.52	−0.04	−0.56	0.29	−0.23	0.30
HD97320	TD	−1.33	0.07	0.44	0.33	−0.11	0.41	−0.03	−0.10
CD-51 4628	low-α	−1.45	−0.04	0.65	0.25	−0.40	0.46	−0.19	0.25
G18-39	high-α	−1.65	0.06	0.32	0.31	−0.01	0.27	−0.05	−0.09

Now the abundances of the heavy elements are analyzed individually, they can be compared to each other.

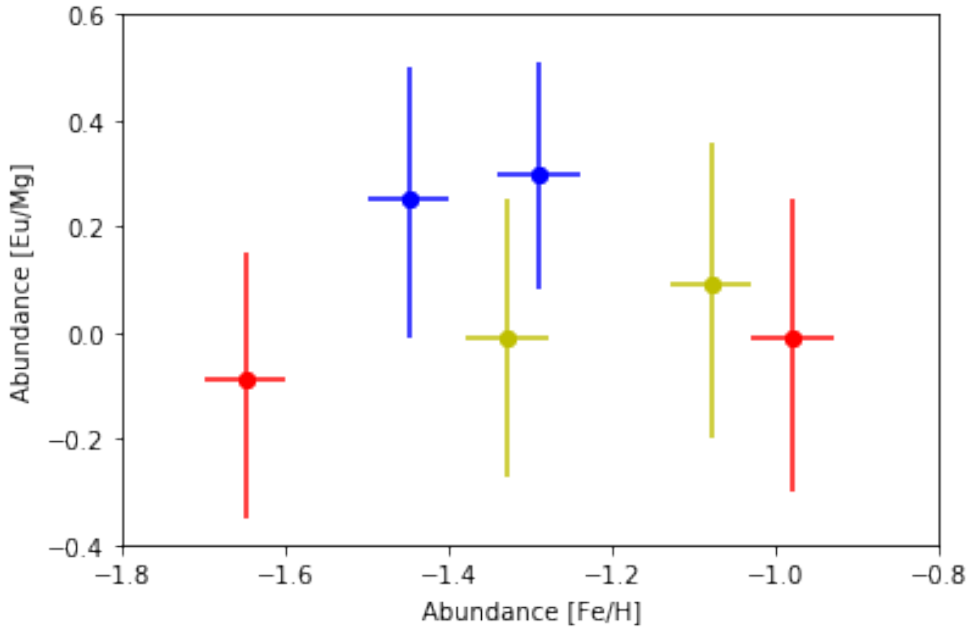

Figure 31: The europium-magnesium abundance ratio for my star sample. Blue are low-α, red are high-α and yellow TD.

From the [Eu/Mg] ratio in Figure 31 the large error bars are very obvious. This is caused by both individual elements having large confidence intervals. However, we can see that the low-α stars appear to have a higher relative abundance than the other stars, indicating more r-process events in their history.

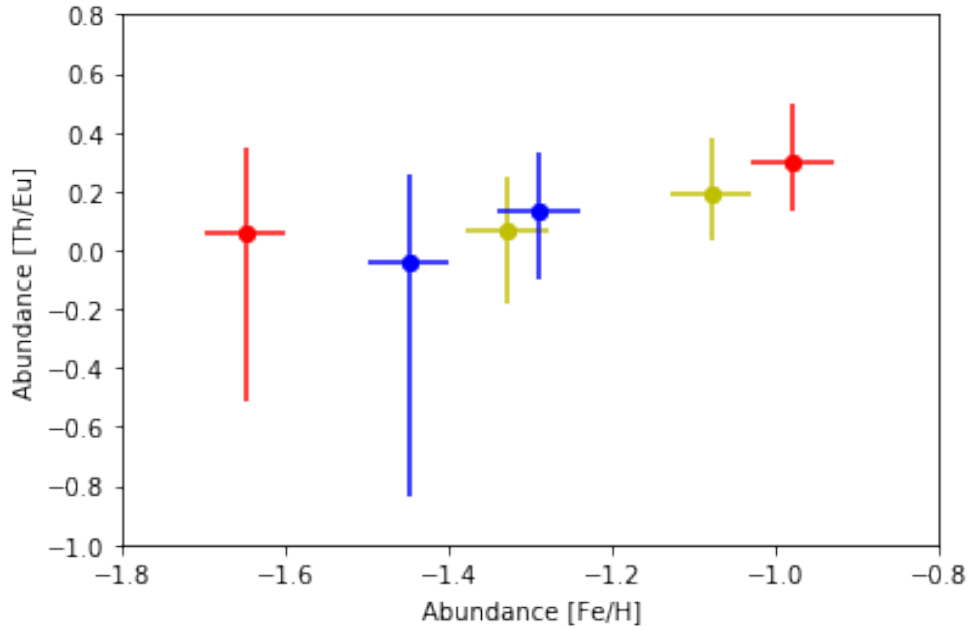

Figure 32: The thorium-europium abundance ratio for my star sample. Blue are low-α, red are high-α and yellow TD.

Like in Figure 27, we observe rather large confidence intervals for the two most metal poor stars, limiting interpretations one can draw from this plot. It seems that there is possibly a slight increasing trend in the abundance ratio as a function of iron. However, the low number of data points as well as the high uncertainty intervals for two of them prevent us from drawing definite conclusions. The different populations also do not show differences in [Th/Eu].

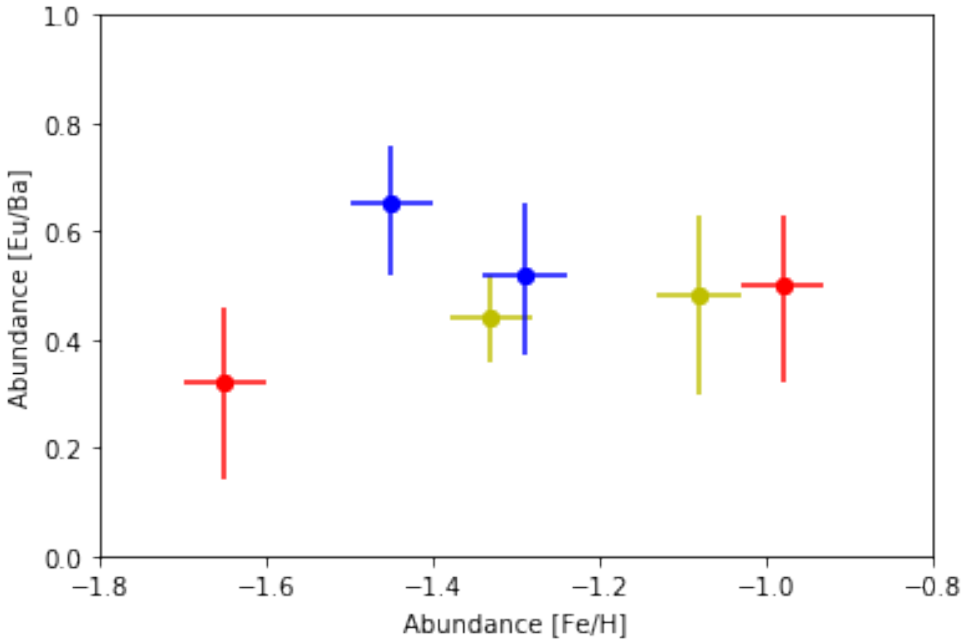

Figure 33: The europium-barium abundance ratio for my stellar sample. Blue are low-α, red are high-α and yellow TD.

In Figure 33, we observe a low ratio for high-α star G18-39, a high ratio for low-α star CD-51 4628, and similar ratio's for the other stars. This indicates that the ratio might be higher for low-α stars in general, but there are not enough data points to draw a definite conclusion.

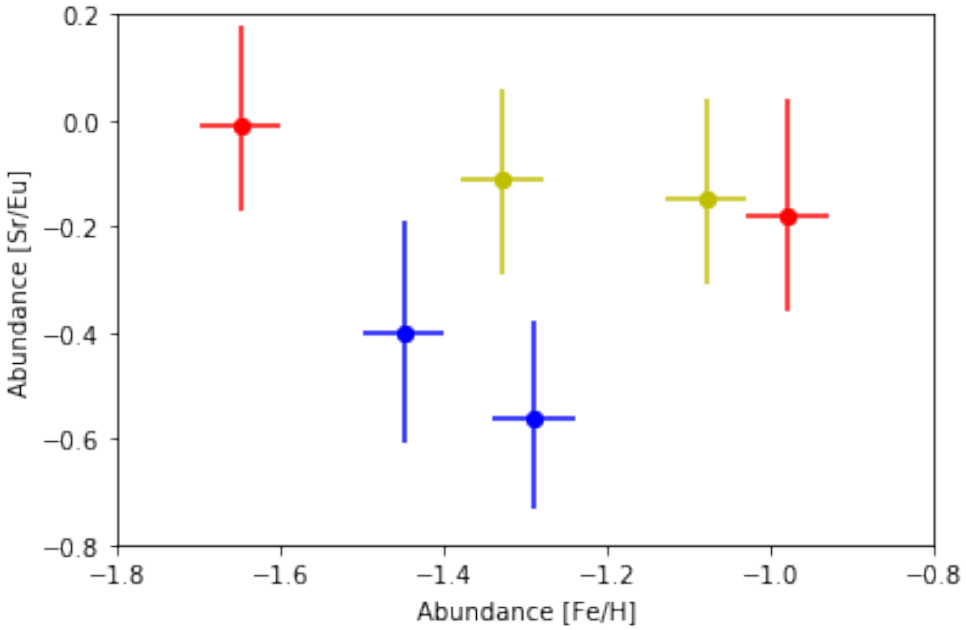

Figure 34: The strontium-europium abundance ratio for my star sample. Blue are low-α, red are high-α and yellow TD.

In Figure 34, one immediately observes that the low-α stars have a significantly lower [Sr/Eu] than the other stars, indicating that the low-α stars have more r-process events in their history. Additionally, there seems to be a decreasing trend in the ratio as a function of the iron abundance.

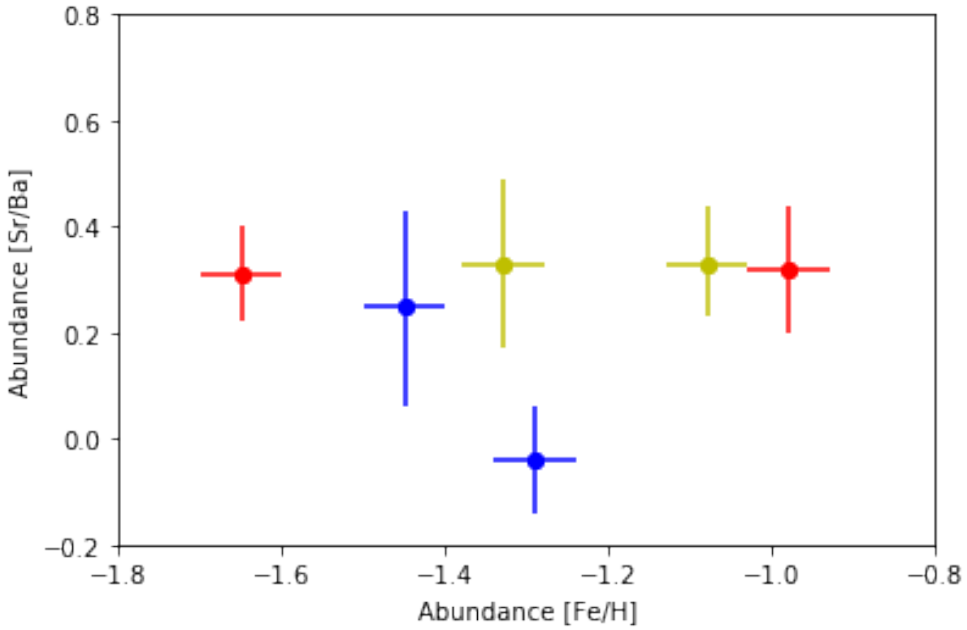

Figure 35: The strontium-barium abundance ratio for my star sample. Blue are low-α, red are high-α and yellow TD.

In figure 35, we observe that the strontium/barium abundance ratio is similar for almost all the stars at around [Sr/Ba] = 0.3. The one exception is HD193901, which has an ratio lower than the others.

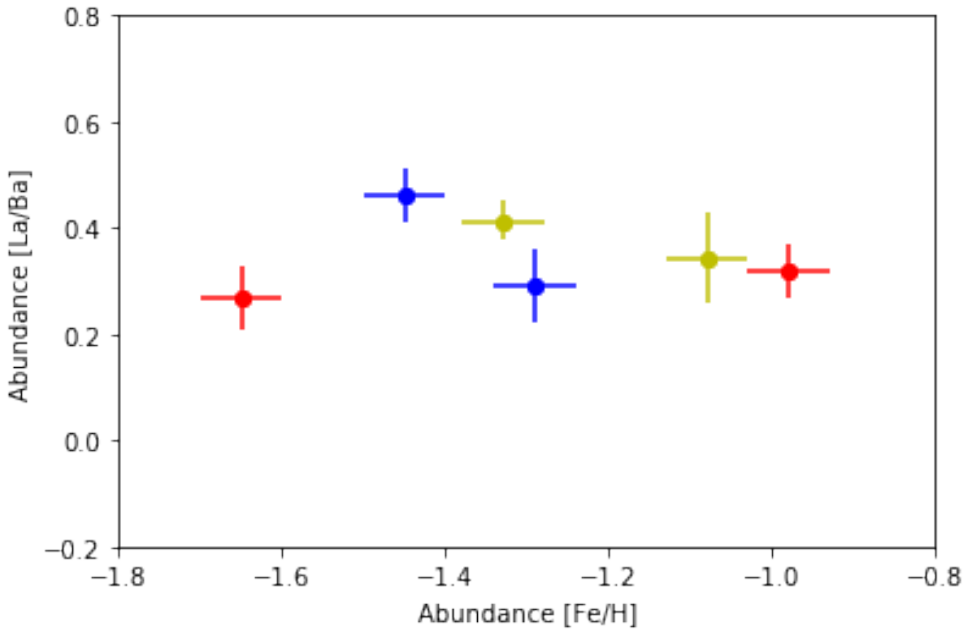

Figure 36: The lanthanum-barium abundance ratio for my star sample. Blue are low-α, red are high-α and yellow TD.

In figure 36, the [La/Ba] abundance ratios seem to be evenly spread around [La/Ba] $\approx$ 0.4. No real trend can be observed, which would have been expected if one of the two elements had more i-process in its history than the other, according to A. Skúladóttir.

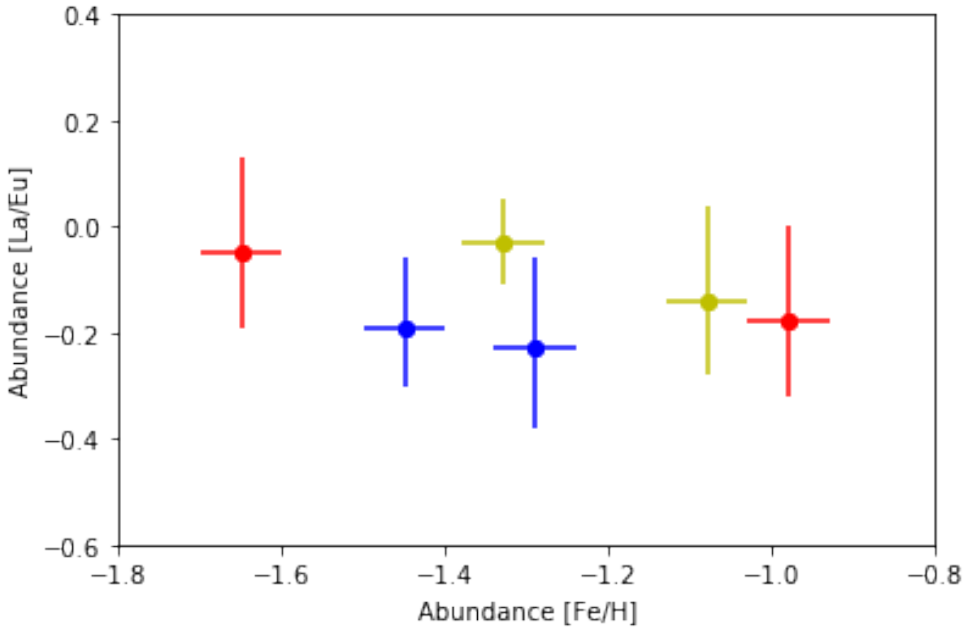

Figure 37: The lanthanum-europium abundance ratio for my star sample. Blue are low-α, red are high-α and yellow TD.

In Figure 37, one observes that [La/Eu] are rather similar for all stars, being somewhat below 0. The low-α stars appear to have a slightly lower abundance ratio that the other stars, and there might be a decreasing trend in the ratio as a function of the iron abundance.

8 Discussion

Some of the heavy elements I measured have already been measured in other papers for the same stars. NS11 [13] measured the barium abundance in all the stars, while Fishlock et al [14] measured the Eu and La abundance for three of the stars. Their results are summarized and compared with my own results in Table 7.

Table 7: Abundance ratios for the sample of stars compared with the observations from the paper by Fishlock et al [14] and NS11 [13]

ID	Class	$[\frac{Fe}{H}]$	$[\frac{Fe}{H}]$ (NS10)	$[\frac{Eu}{Fe}]$	$[\frac{Eu}{Fe}]$ (Fish)	$[\frac{La}{Fe}]$	$[\frac{La}{Fe}]$ (Fish)	$[\frac{Ba}{Fe}]$	$[\frac{Ba}{Fe}]$ (NS11)
HD148816	high-α	−0.98	−0.73	0.34		0.16		−0.16	−0.26
HD76932	TD	−1.08	−0.87	0.45	0.21	0.31	0.03	−0.03	−0.07
HD193901	low-α	−1.29	−1.07	0.49	0.24	0.26	−0.00	−0.03	−0.19
HD97320	TD	−1.33	−1.17	0.27		0.24		−0.17	−0.19
CD-51 4628	low-α	−1.45	−1.30	0.52		0.33		−0.13	−0.16
G18-39	high-α	−1.65	−1.39	0.46	0.26	0.41	0.07	0.14	−0.02

One thing to note before comparing the results is that Fishlock's paper didn't measure the iron abundance on their own. Instead, they simply took the iron abundance from NS10 for granted and used it to calculate the [Eu/Fe] and [La/Fe] abundances. As there is an average difference of 0.21 dex between my observed Fe abundances and those from NS10, we should expect the [Eu/Fe] and [La/Fe] abundances from Fishlock to be that much lower.

When correcting for the difference in iron abundance, the La and Eu abundances of my measurements and Fishlock are rather similar, always being within ± 0.1 dex of each other. This gives further proof of the reliability of my results.

My barium abundances appear to be a bit higher than those from NS11. The difference ranges from 0.02 dex to 0.16 dex. As I only measured a single barium line, although a strong and unblended one, this difference might be a result of an issue with this one line.

In the Fishlock paper, they showed that [Ba/Eu] was lower in low-α stars compared to high-α stars. My re-

sults as shown in Figure 33 agree with this, as the low-α stars have on average a visibly higher Eu/Ba ratio. My results, which can be seen in Figure 26, also agree with their unconfirmed suspicion that low-α stars have a higher europium abundance. However, the difference between the high and low-α stars is rather small in my case.

As can be seen in Figure 31, [Eu/Mg] observed in my stars are on average significantly higher for the low-α stars, albeit with large confidence intervals. This observation is consistent with the observations from Matsuno et al [19], where the Gaia-Encaladus stars were observed to have enhanced [Eu/Mg]. Additionally, as can be observed in Figures 33 and 37 neither the [Ba/Eu], nor the [La/Eu] ratios of my low-α stars are enhanced, which is consistent with the observations from Matsuno et al[19]. In fact, both of those ratios appear to be lower for low-α stars, indicating that my Gaia-Encaladus stars might have even less s-process enhancement than the other halo stars.

In Hansen et al (2018)[21], they observed an average [Th/Fe] = 0.33 (0.38 excluding upper limits) for their sample stars from the Sagittarius dwarf galaxy. However, their standard deviation was high at 0.49 (0.31 excluding upper limits). With the exception of thick disk star HD97320, all my stars have a higher thorium abundance. However, they are also all within one standard deviation of the average, which combined with the high uncertainty in the Th abundance of the lower metalicity stars makes me unable to state with certainty that either my low-α or high-α populations have a higher thorium abundance.

In case of europium, there is more of an indication that my low-α stars might have a higher abundance than the Sagittarius stars. Both of my stars have an Eu abundance that is approximately one standard deviation (0.25) higher than the average Eu abundance of 0.25 in the Hansen paper[21].

The [Ba/Sr] ratios of my stars have, with the exception of star HD193901, an abundance of approximately -0.3, while said HD193901 has an abundance of just above 0. These all fall within the range of values displayed by the stars in the Hansen paper, although on the high side. Unfortunately, as I haven't measured Nd, I can't directly compare my results to their obtained [hs/ls] ratios. However, as the lanthanum abundance of my stars is higher than their average abundance (0.17 with an standard deviation of 0.43), I expect my [hs/ls] abundance ratios to be on average higher than theirs. According to the Hansen paper, this would indicate more metal-poor AGB enrichement in the history of my stars, especially HD193901, while most of the Sagittarius stars are predicted to have more metal-rich AGB enrichement due to their low [hs/ls] ratio's.[21]

My low-α stars also have rather low [La/Eu] ratio's, as can be observed in Figure 36. At the same time, as described earlier, they have a high [hs/ls] ratio, especially HD193901. This might be an indication of i-process in the history of the Gaia-Encaladus dwarf galaxy, as described in the paper by Dardelet et al (2015) [9], although more stars should be measured before drawing definitive conclusions.

8.1 Solar comparison

Using Table 5, we can compare the abundances in the measured stars to our sun. With [Fe/H] between -0.98 and -1.65, the stars are more metal poor than our sun. However, the α-element abundances ([Mg/Fe] & [Ca/Fe]) are higher than solar, even for the low-α stars. However, this is only relative to iron as the absolute abundances are still below solar due to the low metallicity.
For the majority of the stars, the [Sr/Fe] abundance is slightly higher than solar while the [Ba/Fe] abundance is slightly lower than solar, indicating that those stars had more weak s-process events but less strong s-process events in their past compared to the sun.

Both the measured [Eu/Fe] and [Th/Fe] abundances are significantly higher than solar, indicating more r-process events in the history of my stars. The [La/Fe] abundance is also higher than solar, in contrast to fellow 2nd s-process peak element Ba. However, this can be explained as La is not only an s-process element but can also be created by the r-process and i-process.

8.2 Suggestions for further research

The main downside of my research is the low sample size of the stars. Even though I have a lot of information on the individual stars, it is hard to state anything definitive on the whole population if you have only two stars per group. The most I can do is either provide more certainty for conclusions of other people's papers, or point out unusual abundance ratios in my stars and say that it might apply to the whole population. Either way, doing the same research with more stars per group will give my results more certainty and allow us to make definitive statements on the total populations. However, I have to note here that the stars I observed from NS10 are the ones with the best signal-to-noise ratio. Additionally, there are many stars from NS10 that do not have observations in the full 3730-4400 Å wavelength range.

The second improvement that can be made on my thesis is to include more elements. Nd for example has multiple lines in my wavelength range and can be used to compare my [hs/ls] ratios with those from Hansen et al[21]. While the strongest Pb line (4057.807 Å) proved to be hard to measure in my stars due to the nearby Mg and CH lines, it is not impossible if first the CH abundance is carefully measured and taken into account. Additionally, some of the stars have spectra that go more into the blue, which would allow us to measure the stronger lines of the third r-process peak elements like platinum.

Another suggestion for further research is to measure the iron and magnesium abundance of my stars again. As I described earlier, the abundances I obtained from the individual magnesium lines didn't agree with each other, resulting in high uncertainty intervals. Reducing the uncertainty intervals would help to draw more accurate conclusions. Additionally, my observations state that my stars have a metallicity which is significantly (0.21 dex) and consistently lower than the metallicity found by NS10. Therefore, it would be helpful to measure the metallicity of the NS10 stars in the blue part carefully. In this work, we measured Fe to compare our calibration compared to other works. It could be looked at as part of a full analysis of the stellar atmosphere models.

9 Conclusion

In this thesis I measured the abundance of thorium in 6 of the NS10 stars. I also measured the abundance of s-process elements strontium and barium, r-process element europium, as well as lanthanum. The metallicity found in my six stars was approximately 0.21 dex lower than that found in NS10. However, as this was a consistent bias, the calcium and magnesium abundances found (in [x/Fe]) were both within 2 standard deviations of the NS10 abundances.

The low-α population stars, or Gaia-Encaladus stars, are found to have distinct abundances from the high-α and thick disk stars. Their magnesium abundance is lower, while their europium abundance appears to be higher (Especially if measured as [Eu/Mg]. The [Sr/Eu] ratio of the low-α stars is also significantly lower, indicating enhanced r-process abundances in those stars. The low [Eu/La] abundance ratios of the Gaia-Encaladus stars combined with rather high [hs/ls] ratios hint at possible i-process in the history of said galaxy.

My results seem to agree with earlier studies of the NS10 stars, taking into account the metallicity bias. Additionally, the thorium and europium abundance of the Gaia Encaladus stars is within the range displayed by the stars of the Sagittarius dwarf galaxy [21], although higher than average.

Finally, even though the observed stars come from three different populations, it is remarkable that [Th/Fe] and most of their other abundances are remarkably similar.

10 Acknowledgements

I want to thank my supervisors E. Tolstoy and J. Even, as well as Á. Skúladóttir for giving useful feedback and helping me on the way.
I also want to thank D. Sardjan for sharing his deconvolution code and helping me get started with the Turbospec program.
This thesis is based on observations collected at the European Southern Observatory under ESO programmes: 072.B-0179, 076.D-0086, 095.D-0504

References

[1] Iliadis C. *Nuclear Rhyisics of Stars*. Wiley-VCH, 2015.

[2] Cowan J.J. et al. "Origin of the Heaviest Elements: the Rapid Neutron-Capture Process". In: *Rev. Mod. Phys 93, 15002* (2021), pp. 1–96.

[3] Johnson J. *The origin of the solar system elements*. 2017. URL: http://www.astronomy.ohio-state.edu/~jaj/nucleo/.

[4] Schramm D.N. "Electron-capture supernovae as the origin of elements beyond iron". In: *Astrophys. J. 185* (1973), pp. 293–302.

[5] Shinya W. et al. "Electron-capture supernovae as the origin of elements beyond iron". In: *Astrophys. J. 726* (2011), p. L15.

[6] Côté B. et al. "Neutron star mergers might not be the only source of r-process elements in the milky way". In: *ApJ 875* (2019), p. 106.

[7] Truran J.W. et al. "The helium-driven r-process in supernovae". In: *Astrophys. J. 222* (1978), pp. L63–L67.

[8] Banerjee P. et al. "Long, Cold, Early r Process? Neutrino-Induced Nucleosynthesis in He Shells Revisited". In: *Phys. Rev. Lett. 106* (2011).

[9] Dardelet L. et al. "The i-process and CEMP-r/s stars". In: *Proceedings of Science of the conference XIII Nuclei in the Cosmos* (2015).

[10] Bertolli M.G. et al. *Systematic and correlated nuclear uncertainties in the i-process at the neutron shell closure N = 82*. 2013. arXiv: 1310.4578 [astro-ph.SR].

[11] Roskar R. et al. "Galactic Archaeology". In: *Science 338* (2012), pp. 334–335.

[12] Nissan N.E. Schuster W.E. "Two distinct halo populations in the solar neighborhood. Evidence from stellar abundance ratios and kinematics." In: *A&A 511* (2010), p. L10.

[13] Nissan N.E. Schuster W.E. "Two distinct halo populations in the solar neighborhood. Evidence from stellar abundances of Mn, Cu, Zn, Y, and Ba". In: *A&A 530* (2011), A15.

[14] Fishlock C.K. et al. "Sc and neutron-capture abundances in Galactic low- and high-α field halo stars". In: *MNRAS 466* (2017), pp. 4672–4682.

[15] Z.S. et al Ge. "Age of 70 dwarfs of three populations in the solar neigborhood: Considering O and C abundances in stellar models". In: *ApJ 833* (2016), p. 161.

[16] Nissan N.E. Schuster W.E. "Two distinct halo populations in the solar neighborhood. Evidence from stellar ages and orbital parameters." In: *A&A 538* (2012), A21.

[17] Gaia Collaboration et al. "Gaia Data Release 2: Observational Hertzsprung-Russell diagrams". In: *A&A Gaia Data Release 2 special issue* (2018).

[18] Helmi A. et al. "The merger that led to the formation of the Milky Way's inner stellar halo and thick disk". In: *Nature 563* (2018), pp. 85–88.

[19] Matsuno T. et al. "R-process enhancements of Gaia-Enceladus in GALAH DR3". In: *A&A 650* (2021), A110.

[20] Skúladóttir A. et al. "Neutron-capture elements in dwarf galaxies I: Chemical clocks & the short timescale of the r-process". In: *A&A 631* (2019), A171.

[21] Hansen C.L. et al. "Ages and heavy element abundances from very metal-poor stars in the Sagittarius dwarf galaxy". In: *ApJ 855* (2018).

[22] Ji A.P. Freibel A. "From actinides to zinc: using the full abundance pattern of the brightest star in reticulum II to distinguish between different r-process sites". In: *A&A 856* (2018), p. 138.

[23] Cayrel R. et al. "First measurement of Uranium/Thorium ratio in a very old star: Implications for the Age of the Galaxy". In: *ASP Conference Series 245* (2001).

[24] Goriely S. Clairbaux B. "Uncertainties in the Th cosmochronometry". In: *A&A 346* (1999), p. 798.

[25] Yushenko A. et al. "Thorium-rich halo star HD 221170: Futher evidence against the universality of the r-process". In: *A&A 430* (2005), pp. 255–262.

[26] Sansonetti J.E. Martin W.C. *Handbook of Basic Atomic Spectroscopic Data*. 2013. URL: https://www.nist.gov/pml/handbook-basic-atomic-spectroscopic-data.

[27] ESO. *Archives and Catalogues*. 2019. URL: http://www.eso.org/sci/observing/tools/catalogues.html.

[28] Dekker. H. et al. "Design, construction, and performance of UVES, the echelle spectrograph for the UT2 Kueyen Telescope at the ESO Paranal Observatory." In: *SPIE 4008* (2000), pp. 534–545.

[29] Lodders K. *Solar Elemental Abundances*. Oxford University Press, 2019.

[30] J.J. Cowan. "First detection of platinum, osmium and lead in a metal-poor halo star: HD 126238". In: *ApJ 460* (1996), pp. L115–L118.

[31] Alvarez R. Plez B. "Near-infrared narrow-band photometry of M-giant and Mira stars: models meet observations". In: *A&A 330* (1998), pp. 1109–1119.

[32] Gustafsson B. et al. "A grid of MARCS model atmospheres for late-type stars". In: *A&A 486* (2011), pp. 951–970.